

**Thermal Field-Flow Fractionation (Thermal FFF) and Asymmetrical Flow Field-Flow
Fractionation (AF4)
as new tools for the analysis of block copolymers and their
respective homopolymers.**

by

Nyashadzashe Ngaza

*Thesis presented in partial fulfilment of the requirements for the degree
Master of Science (Polymer Science) at the
University of Stellenbosch*



**Supervisor: Prof.Harald Pasch
Faculty of Science
Department of Chemistry and Polymer Science**

December 2014

DECLARATION

I declare that the entire work contained in this thesis is my own, original work and that reproduction and publication thereof by Stellenbosch University will not affect any third party rights and that I have not previously in its entirety or in part submitted it for a degree at any other university.

Nyashadzashe Ngaza

December 2014

"

"

"

"

"

"

"

"

"

"

"

"

"

"

"

"

"

"

"

"

"

"

"

"

"

"Eqr { tki j vÍ "4236"Uvngpdquej "Wpkxgtukv{
Cmłki j w'tgugtxgf "

"

ABSTRACT

Polystyrene-block-poly(ethylene oxide) (PS-b-PEO) copolymers contain a hydrophilic PEO block and a hydrophobic PS block. PS and PEO have different affinities for most organic solvents and as a result, the PS-b-PEO copolymers are difficult to characterize in solution. In order to achieve a complete characterization of their molecular heterogeneity different techniques have been used. Recently FFF has become a cutting edge technology for polymer analysis because it possesses a number of advantages over conventional SEC and other liquid chromatographic techniques. The mild operating conditions allow the analysis of delicate and sensitive complex analytes such as complex polymer assemblies. The ability to analyze polymers with ultrahigh molar masses has also contributed to its significance in the characterization of polymers.

In this study, the FFF behaviour of PS-b-PEO copolymers as well as PS and PEO homopolymers was investigated using Thermal FFF in different organic solvents and AF4. The aim of the study was the correlation of the thermodynamic quality of the solvents and the elution behaviour of the polymers. Unfortunately, PEO homopolymers have been found to interact with the membrane in AF4. Therefore, they were best characterized in organic solvents using Thermal FFF. In contrast to AF4 no specific interactions occurred due to the absence of a membrane. Results for Thermal FFF showed that in all utilized solvents, PS and PEO homopolymers were separated in the direction of increasing molar mass. For PS-b-PEO copolymers the retention in selective (good) solvents for PS was dependent on the molar mass of the PS block in the block copolymer. This was explained by the fact that in poor solvents PEO adopts a collapsed coil conformation while PS is present in extended random coil conformation. Results also showed that polymer retention was dependent on the temperature programme utilized. The fractionations by Thermal FFF indicated that some of the PS-b-PEO copolymer samples contained PS and PEO homopolymers as by-products. After semi-preparative fractionation these homopolymers were qualitatively identified using FTIR spectroscopy.

OPSOMMING

Polistireen-blok-poli(etileenoksied) (PS-b-PEO) ko-polimere bevat 'n hidrofiliese politetileen oksied (PEO) blok en 'n hidrofobiese polistireen (PS) blok. PS en PEO het verskillende affiniteite vir die meeste organiese oplosmiddels, dit bemoeilik die karakterisering van PS-b-PEO ko-polimere in oplossing. Ten einde 'n volledige karakterisering van hul molekulêre heterogeniteit te bepaal moet 'n verskeidenheid van tegnieke gebruik word. Onlangs het veldvloei-fraksionering (FFF) baie grond gewen tov polimeer analise, aangesien dit verskeie voordele het bo tradisionele chromatografiese tegnieke soos grootte-uitsluitingschromatografie (SEC). Die ligte operasionele omstandighede laat die ontleding van 'n verskeidenheid van polimere toe, enige iets van delikate polimeer komplekse tot ultra hoë molekulêre massa.

In hierdie studie is die FFF gedrag van PS-b-PEO ko-polimere asook PS en PEO homopolimere ondersoek met behulp van Termiese FFF(ThFFF) in verskillende organiese oplosmiddels en onsimmetriese vloeiveldvloei-fraksionering(AF4). Die doel van die studie was om die verband tussen die termodinamiese gehalte van die oplosmiddels en die eluering gedrag van die polimere te bepaal. Analise van PEO homopolimere was onsuksesvol aangesien daar interaksie was met die membraan. PEO is dus net geanaliseer in organiese oplosmiddels met behulp van ThFFF, aangesien daar geen membraan is nie. Analise met ThFFF het gewys dat skeiding plaasvind volgens 'n toename in molekulêre massa in organiese oplosmiddels. Vir PS-b-PEO ko-polimere die retensie in selektiewe (goeie) oplosmiddels vir PS was afhanklik van die molekulêre massa van die PS blok in die ko-polimeer. 'n Moontlike teorie is dat die PEO blok 'n ineengestorte spoel struktuur vorm terwyl die PS blok 'n uitgestrekte lukraake vorm aan neem. Resultate het ook getoon dat die polimeer retensie afhanklik was van die temperatuur program wat gebruik is. Die fraksionering deur ThFFF het aangedui dat sommige van die PS-b-PEO kopolimeer monsters bestaan het uit PS en PEO homopolimere as by-produkte. Hierdie is kwalitatief bewys deur analise van die fraksies na fraksionering van die ko-polimere met behulp van FTIR spektroskopie.

ACKNOWLEDGEMENT

Firstly, I would like to thank my supervisor Prof H. Pasch, for his support and guidance throughout my study period. I know your patience was tested a lot at times but you never gave up on me.

Then I would like to thank all the staff at Polymer Science for their help over the past years. Thanks to Polymer Science, NRF and the Zimbabwean government for financial support during this project.

Thanks to all the colleagues in our group for support. Special thanks go to Maggie, Khumo, Helen, Ashwell, Nadine and Pritish.

Last but not least, I would like to thank my family especially my husband (Cleo), my mother (Sharai), brothers Daniel and Kudzi and sisters Tariro and Zviko for all their support throughout these years and who believed in me that I could finish this work.

I would like to thank the Jehovah God for His guidance.

CONTENTS PAGE

DECLARATION.....II

ABSTRACTIII

OPSOMMING..... IV

ACKNOWLEDGEMENT..... V

LIST OF ABBREVIATIONS XIV

LIST OF SYMBOLS XVI

CHAPTER 1: 1

INTRODUCTION AND OBJECTIVES 1

1.1 Introduction 2

1.2 Objectives 3

1.3 References 4

CHAPTER 2: 5

LITERATURE REVIEW 5

2.1 Polystyrene-polyethylene oxide block copolymers (PS-b-PEO)..... 6

2.2 Polymer analysis and characterization techniques 7

2.2.1 General introduction to field-flow fractionation 7

2.2.2 Advantages of FFF sub-techniques (AF4 and Thermal FFF) 9

2.2.3 Principles in FFF 10

2.2.4 Operating modes 11

2.3 Theoretical principles behind field-flow fractionation techniques 12

2.4 Asymmetrical flow field-flow fractionation (AF4) 14

2.4.1 Channel set-up 14

2.4.2 Theoretical principles behind asymmetric flow field-flow fractionation 15

2.4.3 Steps in the AF4 experiment.....	17
2.5 Thermal field-flow fractionation (Thermal FFF).....	18
2.6 Applications of AF4 and Thermal FFF	21
2.7 Detectors.....	24
2.7.1 Refractive index detector (RI)	24
2.7.2 Dynamic light scattering detector (DLS) (zetasizer)	24
2.7.3 Multiangle light scattering (MALLS)	25
2.8 References	27
CHAPTER 3:	30
EXPERIMENTAL	30
3.1 Chemicals	31
3.1.1 Solvents used for thermal field-flow fractionation (THERMAL FFF)	31
3.1.2 Solvents used for asymmetrical flow field-flow fractionation (AF4)	31
3.1.3 Polymer standards.....	31
3.1.4 Copolymers.....	32
3.2 Field-flow fractionation techniques	32
3.2.1 Thermal field-flow fractionation (Thermal FFF) system	32
3.2.2 Asymmetrical flow field-flow fractionation (AF4) system.....	33
3.3 Calibration of the RI and MALLS detectors with PS calibration standards in THF	33
3.3.1 Calibration of the RI detector	33
3.3.2 Calibration of the MALLS detector.....	34
3.4. FTIR-ATR.....	34
CHAPTER 4:	35
RESULTS.AND DISCUSSION	35
4.1 Introduction	36
4.2 Thermal FFF fractionations in chloroform	36
4.2.1 Experimental conditions	36
4.2.2 Fractionation of PS and PEO homopolymers by Thermal FFF	38

4.2.3 Fractionation of PS-b-PEO copolymers by Thermal FFF and comparison with PS and PEO homopolymers.....	41
4.2.4 Qualitative FTIR analysis of the separated components of PS-b-PEO 218 kDa block copolymer	46
4.3 Thermal FFF fractionations in THF	49
4.3.1 Experimental conditions	49
4.3.2 Analysis of PS and PEO homopolymers by Thermal FFF.....	50
4.3.3 Fractionation of PS-b-PEO copolymers by Thermal FFF and comparison with PS and PEO homopolymers	55
4.3.4 Qualitative FTIR analysis of the separated components of PS-b-PEO 218 kDa block copolymer	61
4.4 Thermal FFF fractionations in toluene	62
4.4.1 Fractionation of PS homopolymers by Thermal FFF in toluene.	63
4.4.2 Fractionation of PS-b-PEO copolymers by Thermal FFF and comparison with PS and PEO homopolymers.....	66
4.4.3 Fractionation of PS-b-PEO copolymers and PS and PEO homopolymers by Thermal FFF in toluene using a linear temperature programme.....	69
4.4.4 Fractionation of PS-b-PEO copolymers and comparison to PS and PEO homopolymers.	72
4.5 Analysis of PS-b-PEO copolymers, PS and PEO homopolymers by AF4 coupled to MALLS-RI detection	75
4.5.1 Analysis conditions	75
4.5.2 Analysis of PS-b-PEO copolymers, PS and PEO homopolymers by AF4 in chloroform.....	76
CHAPTER 5:	82
CONCLUSIONS AND FUTURE WORK.....	82
5.1 Conclusions	83
5.2 Future work	85

LIST OF TABLES

Table 2.1	FFF sub-techniques and their respective external forces.....	8
Table 3.1	PS and PEO calibration standards.....	31
Table 3.2	PS-b-PEO block copolymer details according to the manufacturer	32
Table 4.1	dn/dc values for PS-b-PEO copolymers, PEO and PS homopolymers calculated for chloroform.....	38
Table 4.2	Thermal FFF calculated molar masses for PS homopolymers fractionated in chloroform.....	39
Table 4.3	Thermal FFF calculated molar masses for PEO homopolymers fractionated in chloroform	41
Table 4.4	Thermal FFF calculated molar masses for PS-b-PEO copolymers analysed in chloroform	44
Table 4.5	dn/dc values for PS-b-PEO copolymers, PEO and PS homopolymers calculated for THF.....	50
Table 4.6	Molar masses, D and D_T values for PS and PEO determined by Thermal FFF in THF.....	53
Table 4.7	Molar masses, D and D_T values for the block copolymers analysed in THF.....	57
Table 4.8	dn/dc values for PS-b-PEO copolymers, PEO and PS homopolymers calculated for toluene.....	63
Table 4.9	Molar masses, D and D_T for polymers analysed in toluene.....	66

Table 4.10	Molar masses and dn/dc values for PS homopolymers and PS-b-PEO copolymers analysed in toluene using a programmed temperature gradient.....	70
Table 4.11	Molar masses and dn/dc values for PS-b-PEO copolymers, PS and PEO homopolymers in chloroform as determined by AF4.....	76

LIST OF FIGURES

Fig. 2.1	Comparison between molecules analysed by different FFF sub-techniques ¹⁵ .	9
Fig. 2.2	Schematic representation of a FFF channel.....	10
Fig. 2.3	Most frequent FFF modes. different mechanisms of separation for particles of different sizes. (a) normal, (b) steric and (c) hyperlayer mode ²⁹ .	12
Fig. 2.4	Schematic presentation of the AF4 instrumentation setup at Stellenbosch University.	15
Fig. 2.5a	Schematic presentation of the injection step in AF4	17
Fig. 2.5b	Schematic presentation of the focusing step in AF4.....	17
Fig. 2.5c	Schematic presentation of the separating step in AF4	18
Fig. 2.6	Schematic representation of the Thermal FFF instrumentation setup at Stellenbosch University.	19
Fig. 2.7	Schematic presentation of Thermal FFF.....	20
Fig. 4.1	Programmed temperature gradient with T_C 25 °c for polymer analysis.	37
Fig. 4.2	Thermal FFF fractograms in chloroform using a programmed temperature gradient (a) RI signal with molar mass overlaid and (b) MALLS 90° signal with molar mass overlaid. Samples PS 132 kDa, PS 275 kDa and PS 1412 kDa.....	39
Fig. 4.3	Thermal FFF fractograms in chloroform using a programmed temperature gradient (a) RI signal with molar mass overlaid and (b) MALLS 90° signal with molar mass overlaid. Samples PEO 81.9 kDa, PEO 289 kDa and PEO 1015 kDa...	40
Fig. 4.4	Thermal FFF fractograms in chloroform, (a) RI signal with molar mass overlaid and (b) MALLS 90° signal with molar mass overlaid. Samples PEO 81.9 kDa, PS 132 kDa and PS-b-PEO 218 kDa.	42
Fig. 4.5	Thermal FFF fractograms in chloroform, (a) RI signal with molar mass overlaid and (b) MALLS 90° signal with molar mass overlaid. Samples PEO 289 kDa, PS 275 kDa and PS-b-PEO 218 kDa copolymer.	43
Fig. 4.6	Thermal FFF fractograms in chloroform. (a) RI signal with molar mass overlaid and (b) MALLS 90° signal with molar mass overlaid. Samples PS-b-PEO 218 kDa copolymer (F1 and F2).	44
Fig. 4.7	Thermal FFF fractograms in chloroform. (a) RI signal with molar mass overlaid and (b) MALLS 90° signal with molar mass overlaid. samples PEO 1015 kDa, PS 1412 kDa and PS-b-PEO 2280 kDa copolymer.	46

Fig. 4.8 FTIR spectra for (a) PS 132 kDa, fractions (b) F1 and (c) F2 of PS-b-PEO 218 kDa, and (d) PEO 81.9 kDa.47

Fig. 4.9 Thermal FFF fractogram of PS-b-PEO 2280 kDa in chloroform showing the RI (red) and MALLS detector signal at 90° (blue) as a function of retention time. 48

Fig. 4.10 FTIR spectra of (a) Thermal FFF fraction obtained by semi-preparative fractionation of PS-b-PEO 2280 kDa (F3) copolymer, (b) PS homopolymer (c) PEO homopolymer in chloroform.....49

Fig. 4.11 Thermal FFF fractograms of PS homopolymers in THF, (a) RI signal with molar mass overlaid and (b) MALLS 90° signal with molar mass overlaid.51

Fig. 4.12 Thermal FFF fractograms of PS and PEO in THF, (a) RI signal with molar mass overlaid and (b) MALLS 90° signal with molar mass overlaid. Samples PS 275 kDa and PEO 289 kDa.54

Fig. 4.13 Thermal FFF fractograms of PS and PS-b-PEO in tHF. (a) RI signal with molar mass overlaid, (b) MALLS 90° signal with molar mass overlaid. Samples PS-b-PEO 91.5 kDa, PS 29.5 kDa and PS 132 kDa.56

Fig. 4.14 Thermal FFF fractograms in THF, (a) RI signal with molar mass overlaid, (b) MALLS 90° signal with molar mass overlaid. samples: PS 132 kDa and 275 kDa, PEO 289 kDa and PS-b-PEO 91.5 kDa copolymer.58

fig. 4.15 Thermal FFF fractogram of ps-b-peo 218 kDa copolymer in thf. (a) ri signal with molar mass overlaid, (b) malls 90° signal with molar mass overlaid.60

Fig. 4.16 Thermal FFF fractogram of PS-b-PEO 218KDa copolymer showing the UV 254 nm (blue), RI signal (red) and malls detector signal at 90° (black) as a function of retention time in THF.61

Fig. 4.17 FTIR spectra for fractions F1 and F2 (bulk sample) of PS-b-PEO 218 kDa copolymer, PEO 81.9 kDa and PS 132 kDa.....62

Fig. 4.18 Thermal FFF fractograms of PS homopolymers in toluene using a constant temperature gradient, (a) RI signal with molar mass overlaid and (b) MALLS 90° signal with molar mass overlaid. Samples PS 29.5 kDa and PS 132 kDa.....65

Fig. 4.19 Thermal FFF fractograms in toluene using a constant temperature gradient. (a) RI signal with molar mass overlaid and (b) MALLS 90° signal with molar mass overlaid. Samples PS 29.5 kDa, PS 132 kDa and PS-b-PEO 91.5 kDa copolymer.67

Fig. 4.20 Thermal FFF fractograms in toluene using a constant temperature gradient . (a) RI signal with molar mass overlaid and (b) MALLS 90° signal with molar mass overlaid. samples PS 132 kDa and PS-b-PEO 218 kDa copolymer.69

Fig. 4.21 Thermal FFF fractograms in toluene using a programmed temperature gradient. (a) RI signal with molar mass overlaid and (b) malls 90° signal with molar mass overlaid. Samples PS 132 kDa, PS 275 kDa and PS 1412 kDa.....71

Fig. 4.22 Thermal FFF fractograms in toluene using a programmed temperature gradient. (a) RI signal with molar mass overlaid and (b) MALLS 90° signal with molar mass overlaid. Samples PS 132 kDa, PS 275 kDa and PS-b-PEO 218 kDa copolymer.73

Fig. 4.23 Thermal FFF fractograms in toluene using a programmed temperature gradient . (a) RI signal with molar mass overlaid and (b) MALLS 90° signal with molar mass overlaid. Samples PS 1412 kDa and PS-b-PEO 2280 kDa copolymer. .74

Fig. 4.24 AF4 fractograms in chloroform (a) RI signal with molar mass overlaid and (b) MALLS 90° signal with molar mass overlaid. Sample PEO 289KDa.77

Fig. 4.25 AF4 fractograms in chloroform (a) RI signal with molar mass overlaid and (b) MALLS 90° signal with molar mass overlaid. Samples PS 275 kDa and PS-b-PEO 218 kDa copolymer.....79

Fig. 4.26 AF4 fractograms in chloroform (a) RI signal with molar mass overlaid and (b) MALLS 90° signal with molar mass overlaid. Samples PEO 1015 kDa, PS-b-PEO 2280 kDa copolymer and PS 1412 kDa.80

LIST OF ABBREVIATIONS

ACN	acetonitrile
AcFFF	acoustic field-flow fractionation
AF4	asymmetric flow field-flow fractionation (room temperature)
BCP	Block copolymers
CCD	Chemical composition distributions
Da	Dalton
DEP-FFF	dielectrophoretic field-flow fractionation
DLS	dynamic light scattering
DMF	N,N-Dimethylformamide
dn/dc	specific refractive index increment
DV	differential viscometer
EIFFF	electrical field-flow fractionation
ELSD	evaporative light scattering detector
EO	ethylene oxide
FFF	field-flow fractionation
FIFFF	flow field-flow fractionation
FTIR	Fourier-transform infrared spectroscopy
GrFFF	gravitational field-flow fractionation
KDa	KiloDalton
MgFFF	magnetic field-flow fractionation
MALLS	multi-angle laser light scattering
MMD	Polymer molar mass distributions

M_n	number average molecular weight
MS	mass spectroscopy
M_w	weight average molecular weight
PEO	poly(ethylene oxide)
PS	polystyrene
PMMA	poly(methyl methacrylate)
PI	polyisoprene
PS-b-PEO	polystyrene-block-poly(ethylene oxide) copolymer
PEO-b-PCL	poly(ethylene oxide)-block-caprolactone copolymer
PS-b-PI-b-PS	polystyrene-block-polyisoprene-block-polystyrene copolymer
QELS	quasielastic light scattering
RI	refractive index
SEC	size exclusion chromatography
SdFFF	sedimentation field-flow fractionation
Thermal FFF	thermal field-flow fractionation
THF	tetrahydrofuran
UV	ultraviolet

LIST OF SYMBOLS

A_2	second virial coefficient
C	concentration of analyte
d	diameter of molecule/particle
D	diffusion coefficient
D_h	hydrodynamic diameter
dc/dx	change in concentration over the mean layer thickness
D_T	thermal diffusion coefficient
dt/dx	temperature drop between hot and cold walls
F	force field applied perpendicular to the inlet flow
G	gravitational force
J	net flux of energy
K	Boltzmann constant
K^*	optical constant
K	distribution coefficient
L	mean layer thickness
M	molar mass
M'	effective mass
N_a	Avogadro's number
n_o	refractive index of the mobile phase
$P(\theta)$	particle scattering function
Q	scattering vector
R	retention ratio
R_h	hydrodynamic radius
R_θ	Rayleigh ratio
T	temperature
T_c	cold wall temperature
T_h	hot wall temperature
t_o	retention time of an unretained component
t_r	retention time of analyte
U	flow induced field
V_{out}	detector flow rate

v_c	flow rate of the cross flow
V_e	elution volume
V_o	volume of the channel (FFF)
W	width or thickness of the channel
W	weight fraction
ΔT	change in temperature
H	viscosity of mobile phase
Λ	retention parameter

Chapter 1:

Introduction and Objectives

1.1 Introduction

Block copolymers (BCPs) are composed of two or more chemically distinct, polymer blocks covalently bound together. The complex structure of BCP materials leads to a variety of useful properties. Many industrial applications for BCPs as thermoplastic elastomers, foams, adhesives have been around for a very long time¹. Amphiphilic block and graft copolymers are examples of BCPs which consist of hydrophilic and hydrophobic parts. An interesting feature of block copolymers is that their homopolymer blocks retain their individual properties when they are used in different applications. These have become subjects of numerous studies on their solution, solid state, and surface properties². These copolymers have complex distributions in molar mass and chemical composition. They may contain their respective homopolymers as by-products. It is therefore crucial to characterize the chemical composition, molar mass distributions of copolymers as well as their behaviour in different organic solvents. These properties impact on the performance of products made from the copolymers^{1, 3-6}.

Size-exclusion chromatography (SEC) is well known for the determination of molar mass distributions³. The methods for determining chemical composition distributions are liquid chromatography, mass spectrometry and the hyphenation of these techniques^{3, 4}. Another hydrodynamic method, field-flow fractionation (FFF) has become popular in the analysis of chemical composition, molar mass distribution and elution behaviour of polymers⁴⁻⁸. FFF offers working conditions that are conducive for the analysis of sensitive and complex molecules. In FFF ultrahigh molar mass polymers can be analysed due to the absence of a stationary phase; this helps to minimize sample loss due to adsorption. The most popular FFF sub-techniques are asymmetric flow field-flow fractionation (AF4) and thermal field-flow fractionation (Thermal FFF)⁵⁻⁸. In AF4 separation is based on different hydrodynamic sizes. AF4 has been used to characterize size distributions of copolymers⁴. Thermal FFF is a powerful tool for both separation and characterization of polymer molar mass distributions (MMD) and chemical composition distributions (CCD)⁹⁻¹⁴. Thermal FFF has been used to characterize homopolymers in different organic solvents¹⁴⁻¹⁶. The chemical composition and molar mass of copolymers has also been investigated using Thermal FFF^{7, 10, 17}.

In our study non-selective and selective solvents for PS and PEO were used in AF4 and Thermal FFF to investigate the FFF behaviour of these homopolymers and compare them to the behaviour of PS-b-PEO copolymers. FTIR spectroscopy was used to obtain qualitative information about the chemical composition of the components separated by Thermal FFF.

1.2 Objectives

- Find suitable common solvents and selective solvents to dissolve PS, PEO and PS-b-PEO
- Characterise the molecular heterogeneity of PS-b-PEO copolymers in selected solvents
- Determine molar masses of PS, PEO and PS-b-PEO in common solvents and selective solvents.
- Determine ordinary diffusion coefficients (D) of PS, PEO and PS-b-PEO in different solvents.
- Determine thermal diffusion coefficients (D_T) of PS, PEO and PS-b-PEO in different solvents so as to quantitatively analyse separation and retention of polymers in Thermal FFF.
- Characterize PS, PEO and PS-b-PEO in different solvents using AF4.

1.3 References

1. Darling, S. B. *Prog. Polym. Sci.* **2007**, 32, (10), 1152–1204.
2. Caldérara, F.; Hruska, Z.; Hurtrez, G.; Lerch, J. P.; Nugay, T.; Riess, G. *Macromolecules* **1994**, 27, (5), 1210–1215.
3. Philipsen, H. J. A. *J. Chromatogr., A* **2004**, 1037, 329–350.
4. Ehrhart, J.; Mingotaud, A. F.; Violleau, F. *J. Chromatogr., A* **2011**, 1218, 4249–4256
5. Williams, S. K. R.; Runyon, J. R.; Ashames, A. A. *Anal. Chem.* 83, (3), 634–642.
6. Runyon, J. R.; Williams, S. K. R. *J. Chromatogr., A* **2011**, 1218, (39), 7016–7022.
7. Runyon, J. R.; Williams, K. S. R. *J. Chromatogr., A* **2011**, 1218, (38), 6774–6779.
8. Messaud, F. A.; Sanderson, R. D.; Runyon, J. R.; Otte, T.; Pasch, H.; Williams, K. S. R. *Prog. Polym. Sci.* **2009**, 34, 351–368.
9. Williams, K. S. R.; Shiundu, P. M.; Calvin Giddings, J. *Colloids Surf., A* **1995**, 105, 243–250.
10. Batten, C.; Hoyos, M.; Martin, M. *Chromatographia* **1997**, 45, (1), 121–126.
11. Hiller, W.; van Aswegen, W.; Hehn, M.; Pasch, H. *Macromolecules* **2013**, 46, (7), 2544–2552.
12. Shiundu, P. M.; Calvin Giddings, J. *J. Chromatogr., A* **1995**, 715, (1), 117–126.
13. Thompson, G. H.; Myers, M. N.; Giddings, J. C. *Anal. Chem.* **1969**, 41, (10), 1219–1222.
14. Van Asten, A. C.; Kok, W. T.; Tijssen, R.; Poppe, H. *J. Polym. Sci., Part B: Polym. Phys.* **1996**, 34, (2), 283–295.
15. Sisson, R. M.; Giddings, J. C. *Anal. Chem.* **1994**, 66, (22), 4043–4053.
16. Giddings, J. C.; Caldwell, K. D.; Myers, M. N. *Macromolecules* **1976**, 9, (1), 106–112.
17. Jeon Sun, J.; Schimpf M. E., Cross-Fractionation of Copolymers Using SEC and Thermal FFF for Determination of Molecular Weight and Composition. In *Chromatography of Polymers*, American Chemical Society: 1999; Vol. 731, pp 141–161.

Chapter 2:

Literature review

2.1 Polystyrene-polyethylene oxide block copolymers (PS-b-PEO)

PS-b-PEO copolymers are amphiphilic in nature¹. Amphiphilic copolymers contain hydrophobic and hydrophilic segments in the same molecules². The different polymer segments usually have different affinities for different solvents. Polyethylene oxide (PEO) is a hydrophilic, biocompatible, non-toxic polymer soluble in water and many types of organic solvents³. In most cases polyethylene oxide (PEO) is the hydrophilic block because of its good properties mentioned above, while alkyl, aryl alkyl, poly(ether), poly(ester), poly(styrene) blocks, etc. are commonly the hydrophobic blocks^{1,3-5}.

One interesting aspect of amphiphilic polymers is the wide variability of the chemical structures of the polymers². Amphiphilic block copolymers show typical self-assembly and adsorption behaviour similar to conventional low molar mass surfactants⁵. These block copolymers usually form micelles in liquids that are good solvents for one block but poor solvents for the other block⁶⁻⁸. The micellization process and the structural parameters of the micelles are influenced by composition, structure and molar mass of the copolymer, interactions between the copolymer blocks and the solvent, copolymer concentration, temperature, and preparation methods².

There are many polymerization techniques useful for the preparation of block copolymers. These include covalent coupling of two different polymeric chains^{9, 10}, sequential living anionic polymerization and many others. The PS-b-PEO copolymers in this study were synthesized by sequential living anionic polymerization of styrene and ethylene oxide^{1, 11}. This technique involves living or controlled polymerization of monomer A followed by the living or controlled polymerization of monomer B. After consumption of monomer B, the chains are terminated by some external agent. Living anionic polymerisation is most often used as it gives a highly controlled end product, with control over the molar mass, end groups, composition and chain architectures^{9,10}.

In the sequential living anionic polymerization of styrene and ethylene oxide, styrene is typically polymerized at -78°C in tetrahydrofuran (THF) using cumyl potassium as initiator. After 1 h, an aliquot is taken to recover the polystyrene precursor for monitoring purposes.

Ethylene oxide (EO) is then cryodistilled into the reactor. At this stage, the orange colour of the solution changes to a pale yellowish colour. After raising the temperature to 40°C, the reaction is continued for 2 days to complete the polymerization of the second monomer. The polymerization is terminated by addition of methanol. The PS-*b*-PEO copolymer formed is isolated by precipitation in hexane^{1,11}.

2.2 Polymer analysis and characterization techniques

In order to achieve a complete characterisation of the complex polymeric structures, it is best to first use a separation technique to fractionate the polymer into more homogeneous fractions. The characterization of these complex polymeric materials requires accurate analytical techniques that address the various parameters of molecular heterogeneity. The parameters include chemical composition, molar mass, functionality type and molecular topological distributions. Accurate knowledge about the different distributions is very important since they influence the processing and application properties to a large extent. The correct analysis of complex polymers which are heterogeneous in more than one distribution has become an interesting subject of research to many polymer scientists. In this study different field-flow fractionation (FFF) sub-techniques have been utilized for the characterization of PS-*b*-PEO copolymers and their respective homopolymers.

2.2.1 General introduction to field-flow fractionation

Field-flow fractionation was first introduced by J. Calvin Giddings in 1966. Field-flow fractionation (FFF) consists of a family of separation methods for particles and macromolecules¹⁴. Like chromatography, FFF is an elution based technique with differential flow displacement of samples. In FFF separation is based on an applied gradient or field of force, like in ultracentrifugation and electrophoresis¹⁵. The field is applied along an axis perpendicular to the flow axis¹⁶. This brings about the differential elution of macromolecular components from a thin ribbon-shaped channel, which requires no stationary phase and contains no packing^{17, 18}. FFF can also be defined as an elution based chromatography-like method in which the separation is carried out in a single liquid phase¹⁹. In FFF, the field

works together with the flow pattern in the channel to achieve separation. The name field-flow fractionation recognizes this underlying duality¹⁷. Due to the high aspect ratio of the FFF channel a laminar parabolic flow profile develops, with flow velocity increasing from near zero at the channel walls to a maximum at the centre of the channel¹⁹.

Table 2.1 FFF sub-techniques and their respective external forces

Field (force)	Field-flow fractionation (FFF) sub-technique
1. Additional flow	Flow (FIFFF)
2. Temperature gradient	Thermal (Thermal FFF)
3. Electrical potential	Electrical (EIFFF)
4. Centrifugal force	Sedimentation (SdFFF)
5. Gravitational force	Gravitational (GrFFF)
6. Dielectrophoretic field	Dielectrophoretic (DEP-FFF)
7. Acoustic wave	Acoustic (AcFFF)
8. Magnetic field	Magnetic (MgFFF)

The sub-techniques of FFF are named according to the kind of field employed, see Table 2.1¹⁶. Analyte retention and separation in these different FFF techniques arise as a result of different properties such as size, thermal diffusion, chemical composition, charge, density, mass and magnetic susceptibility¹⁷. This makes FFF uniquely suitable to separate and characterize polymers, powders, emulsions, bioparticles, and many additional building blocks of modern synthetic and natural materials^{17, 19}(see Fig. 2.1).

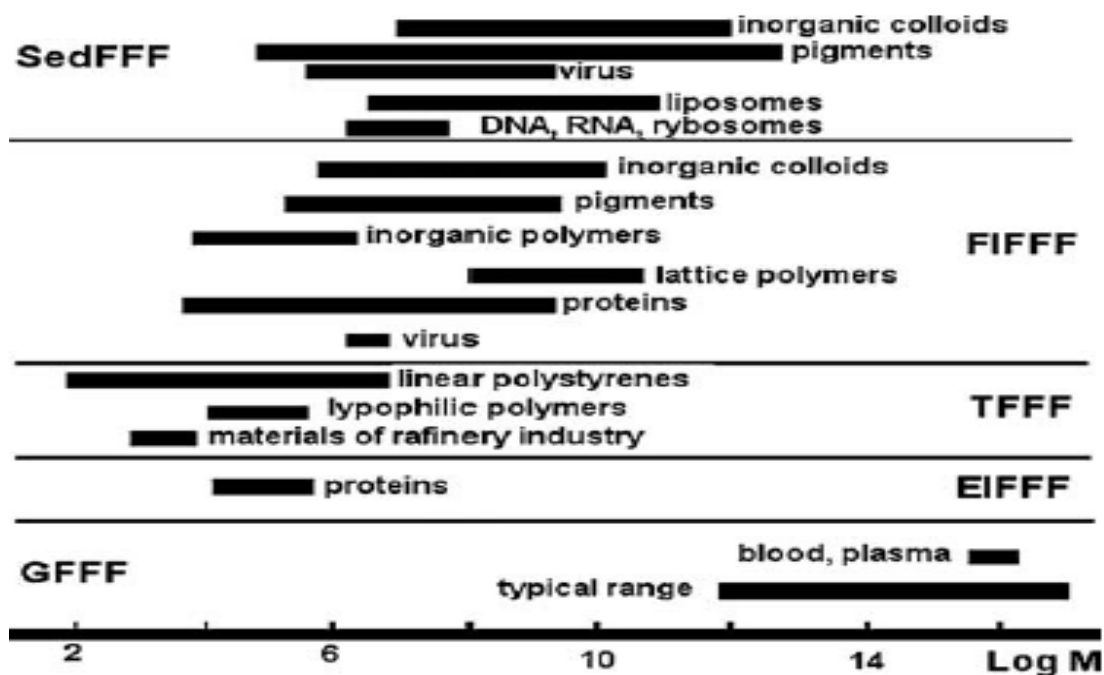


Fig. 2.1 Comparison between molecules analysed by different FFF sub-techniques¹⁵

2.2.2 Advantages of FFF sub-techniques (AF4 and Thermal FFF)

FFF has overcome some of the common limitations of traditional chromatographic techniques for polymer analysis in several ways listed below that has led to its popularity.

- There is no stationary phase in the channel; therefore, there is no sample loss due to adsorption to the stationary phase¹⁹⁻²¹.
- The upper molar mass limit of AF4 extends to the 10^9 Da and micron-size particles¹⁹.
- The absence of the stationary phase minimizes shear degradation of the analytes^{15, 17}.
- FFF can characterize a wide size range of particles from 1 nm to $100\ \mu\text{m}$ ^{15, 20}.
- Complex samples with broad size distributions, heterogeneous mixtures or strongly interacting systems can be analysed in one measurement because of the physical simplicity and stability of FFF¹⁵.

- The conducive operating conditions allow the analysis of fragile and sensitive analytes^{15, 19}.

FFF techniques can characterize even very complex systems with broad size distributions, heterogeneous mixtures or strongly interacting systems. No other fractionating technique can cover about 5 orders of magnitude of particle sizes that have complex distributions^{17, 22}.

2.2.3 Principles in FFF

The separation of the sample takes place inside a narrow ribbon-like channel. This channel is composed of a thin piece of sheet material (usually 70–300 μm thick Mylar or polyimide) known as the spacer in which a channel is cut. The spacer is usually clamped between two highly-polished surfaces parallel to each other through which a force can be applied so as to achieve separation^{17, 19, 22-24}. The actual configuration of the spacer varies with the type of field being utilized. A carrier liquid is pumped through this channel from the inlet, where the sample is injected, to the outlet, to which a detector is connected. Inside the channel, a parabolic flow profile (laminar Newtonian flow) is established as in a capillary tube. Interaction of the solutes with the field concentrates them at one of the channel walls, called the accumulation wall²⁵⁻²⁸ see Fig. 2.2. The elution order of the analytes is determined by the mode of operation being utilized.

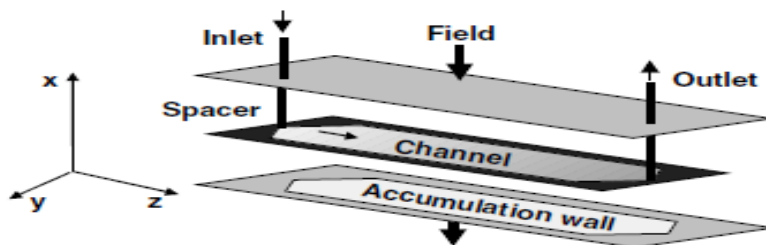


Fig. 2.2 Schematic representation of a FFF channel.

2.2.4 Operating modes

FFF utilizes different operating modes which determine the elution order of the analytes along with other separation characteristics such as selectivity and resolution¹⁷. There are different modes of separation used in field-flow fractionation (FFF) techniques. However, the modes most commonly used are the normal (Brownian) mode, steric mode and the lift hyperlayer mode^{17, 19, 21, 23}.

Normal mode: The normal mode (based on Brownian motion of the analyte in the channel) is for analytes with sizes smaller than 1 μm (macromolecules and submicrometer particles). Smaller component populations diffuse faster and accumulate in regions of faster streams of the parabolic velocity profile and elute earlier than larger components^{17, 19, 21, 22, 29, 30} (see Fig. 2.3a.)

Steric mode: The steric mode considers particles greater than 1 μm in diameter. In this case diffusion becomes negligible and the normal mode mechanism no longer applies. Small particles can approach the accumulation wall more closely than large particles and thus the former's centre of mass is in the slower flowing streamlines of the parabolic flow profile. This elution mode is controlled by the physical (steric) barrier of the accumulation wall, so it is called 'steric', see Fig. 2.3b. The elution order in steric mode is from largest to smallest molecules/particles^{17, 19, 29}.

Lift or hyperlayer mode: The lift or hyperlayer mode is one in which lift forces become large enough to drive sample components to higher velocity streams located more than one particle radius from the accumulation wall. This can happen when the opposing field forces become weak enough. These hydrodynamic lift forces (Fig. 2.3c) occur when high flow velocities are used. The elution order is the same as in the steric mode^{17, 19, 29, 30}.

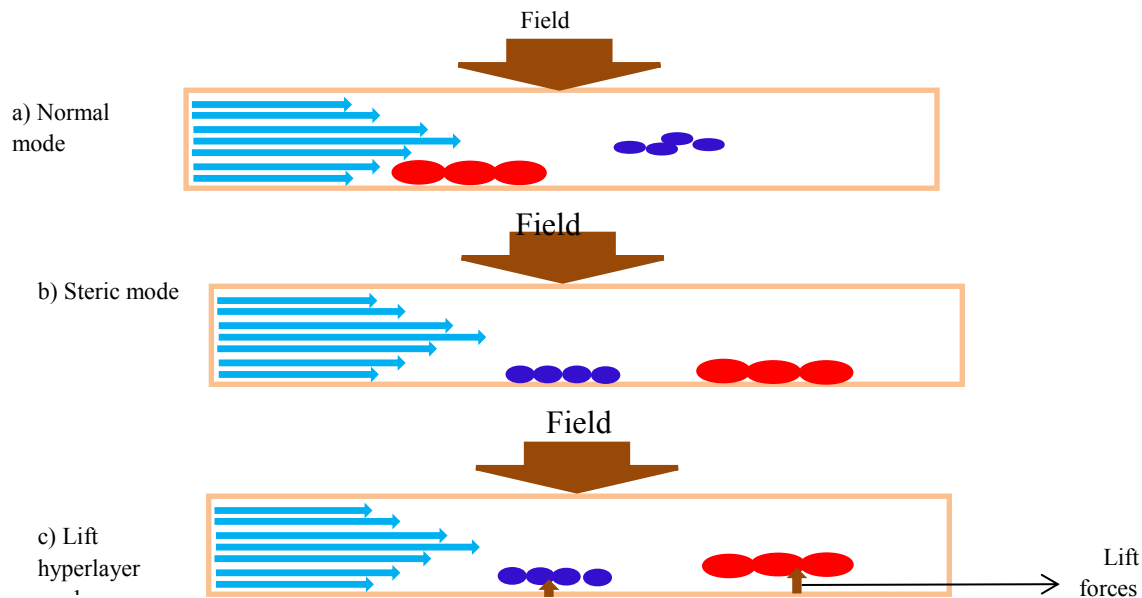


Fig. 2.3 Most frequent FFF modes. Different mechanisms of separation for particles of different sizes. (a) Normal, (b) steric and (c) hyperlayer mode²⁹.

2.3 Theoretical principles behind field-flow fractionation techniques

In FFF the field or force is opposed by sample diffusion processes and therefore sample concentration c (relative to the wall concentration c_0) approaches an exponential function of the mean layer thickness x remote from the accumulation wall²²

$$c(x) = c_0 e^{\left(-\frac{U}{D}\right)x} \quad (1)$$

where U represents the drift velocity of the sample induced by the external field. The diffusion coefficient D can be related to the frictional coefficient by means of the Stokes–Einstein relationship

$$D = \frac{KT}{f} \quad (2)$$

where K is Boltzmann's constant and T is the temperature. The drift velocity U is correlated to the force F , which is exerted on the sample, by $U = F/f$. Different terms are substituted for

F depending on the type of field that is employed. Then the diffusion coefficient becomes $D = [KT(U/F)]$. The mean sample-wall distance I, derived by $I = D/U$ leads to

$$I = \frac{KT}{f} \quad (3)$$

The mean layer thickness I of the sample cloud can also be defined as the distance from the accumulation to the centre of mass of sample zone.

Eq. (3) can be extended by the dimensionless parameter λ , leading to

$$\lambda = \frac{I}{w} = \frac{KT}{Fw} \quad (4)$$

w is the channel thickness, force F will vary depending on which FFF technique is used. The dimensionless retention parameter λ is directly related to physicochemical parameters of the retained components and it also links theory to experiment as will be discussed below through the retention ratio R or the retention time. The retention of an analyte can be described by a retention ratio R. R can be described solely by the dimensionless retention parameter λ .

$$R = 6\lambda \left(\coth \frac{1}{2\lambda} - 2\lambda \right) \quad (5)$$

R can also be described in terms of retention time in FFF and is related to the ratio of the retention time of an unretained component (t_0) the retention time of the solute (t_r) and is defined by

$$R = \frac{t_0}{t_r} = 6\lambda \left(\coth \frac{1}{2\lambda} - 2\lambda \right) \quad (6)$$

For λ values less than 0.02, R can be calculated with an error of ~5% using the 6λ approximation. Alternatively the retention ratio can be expressed as

$$R = \frac{t_0}{t_r} = \frac{V_0}{V_r} = 6\lambda \quad (7)$$

where V_0 is the volume of the FFF channel and V_r is the retention volume.

In this study asymmetrical flow field-flow fractionation (AF4) and thermal field-flow fractionation (Thermal FFF) will be used to separate and characterize the FFF behaviour of complex PS-b-PEO block copolymers and their respective homopolymers in different single solvents.

2.4 Asymmetrical flow field-flow fractionation (AF4)

Flow field-flow fractionation consists of two sub-techniques namely asymmetrical flow field-flow fractionation (AF4) and symmetrical flow field-flow fractionation (FIFFF). The single channel inlet flow is split into the axial flow and the cross-flow (field). One of the main differences between AF4 and FIFFF lies in the channel construction i.e. AF4 makes use of only one permeable wall whereas FIFFF has two permeable walls^{17, 19, 23, 31, 32}.

2.4.1 Channel set-up

The accumulation wall comprises of a ceramic frit covered by an ultrafiltration membrane. The membrane is usually made from cellulose derivatives, poly(ether)sulfone, polycarbonate and many others^{19, 33}. The membrane prevent samples from leaving the channel with the cross flow, therefore its cut-off properties crucially influence potential sample loss and recovery. The ultrafiltration membrane allows the loss of axial flow as the carrier liquid is transported along the channel. This leads to a continuous decrease in the flow velocity of the axial flow, as it approaches the outlet of the rectangular channel^{17, 19, 23}.

The trapezoidal channel geometry shown in Fig. 2.4 was designed in order to compensate these effects^{17, 23, 31}. The trapezoid has a channel breadth that decreases towards the outlet. The advantage of the trapezoidal design is that the axial flow velocity is maintained despite the loss of flow through the membrane. This also reduces the peak dilution as compared to a rectangular channel¹⁷.

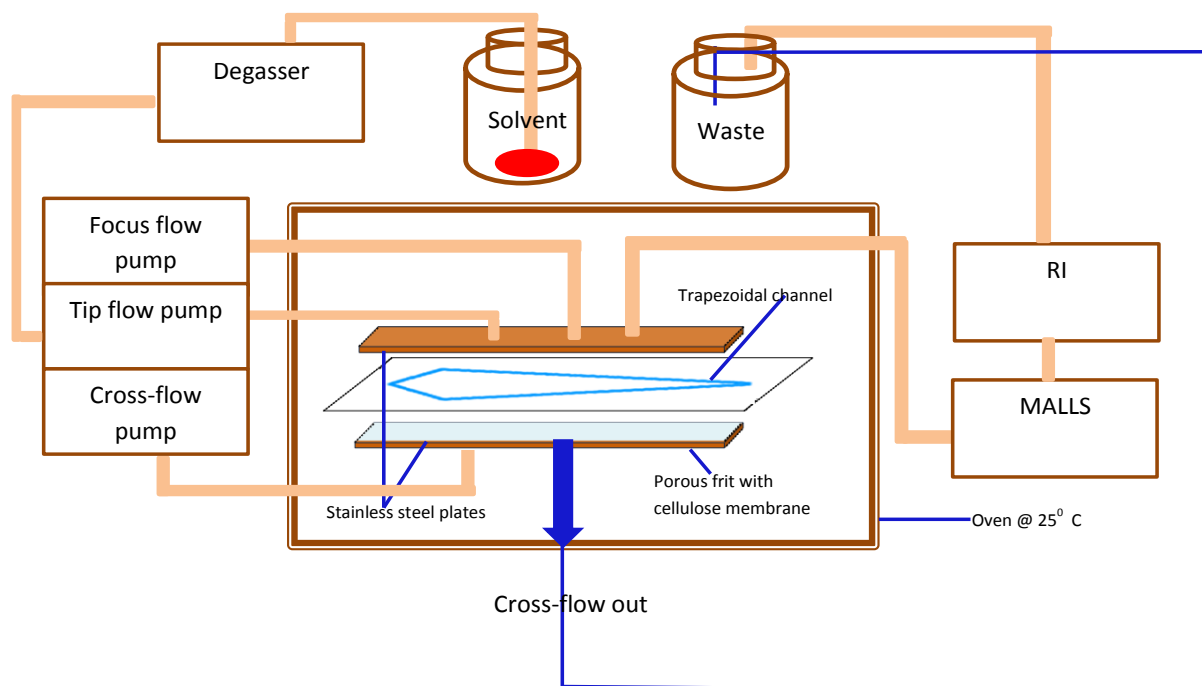


Fig. 2.4 Schematic presentation of the AF4 instrumentation setup at Stellenbosch University.

2.4.2 Theoretical principles behind asymmetric flow field-flow fractionation

The theoretical principles behind AF4 are complicated by the asymmetrical channel design and trapezoidal channel geometry, which are associated with non-uniform flow velocities. In theory it is assumed that the cross flow velocity at any given point is much smaller than the average longitudinal flow velocity thus resulting in parabolic flow along the channel. The pressure drop along the channel is required to be much smaller than that across the accumulation wall in order to ensure a homogeneous permeation of the carrier liquid²³. The cross flow velocity is given by Equation 8

$$U = -|u_0| \left(1 - \frac{3x^2}{w^2} + \frac{2x^3}{w^3} \right) \quad (8)$$

where u is the transverse flow velocity at any point x above the accumulation wall, U_0 is the cross flow velocity at the accumulation wall, and w is the channel thickness, which is the distance between the accumulation wall and the upper wall. The negative sign accounts for

the negative direction of the cross flow along the coordinate axis x . The axial flow velocity at any point z along the channel is given by the linear relationship given in Equation 9

$$\langle V \rangle = \langle V_0 \rangle - \frac{|U_0|}{w} z \quad (9)$$

where $\langle v \rangle$ is the axial flow velocity at the channel inlet. This shows that v decreases linearly along the channel at a rate determined by the cross flow velocity U_0 at the accumulation wall. Another dimensionless parameter is zone thickness known also as the retention parameter λ , which is defined as the ratio $(1/w)$. This represents the degree of zone compactness relative to the channel thickness as well as the volume fraction of the sample layer. The retention parameter is a measure of the extent of the interaction between the field force and the sample components. For general FFF systems, this can be expressed as shown in equation 4.

The calculation of the retention ratio in AF4, unlike for the other FFF forms requires void time (t_0) measurements. The void time is the time it would take an unretained analyte to travel through the channel. Z is the distance from the inlet to the focusing point, V_c the cross flow, V_{out} the outlet flow rate or the axial flow rate, V_0 the void volume and y the area excluded by the tapered inlet end. The equation is shown below

$$t_0 = \frac{V_0}{V_c} \ln \left(1 + \frac{V_0}{V_{out}} \left(1 - \frac{A(z) - y}{A_{out}} \right) \right) \quad (10)$$

$A(z)$ is the area of the accumulation wall from the inlet up to z . When given parameters t_0 , V_c , V_0 , and the experimentally assessed t_r , the diffusion coefficient D can be obtained directly via Equation 11

$$D = \frac{t_0 V_c w^2}{6 t_r V_0} \quad (11)$$

The hydrodynamic diameter d_H of the sample specimen can also be assessed using Equation 12 where η is the solvent viscosity:

$$d_H = \frac{2kTV_0}{\pi\eta V_c w^2} t_r \quad (12)$$

2.4.3 Steps in the AF4 experiment

AF4 experiments are divided into three stages namely sample injection, sample focusing/relaxation, and the separation step¹⁷.

Injection: During sample injection the sample is delivered to the channel see Fig. 2.5a^{17, 22}.

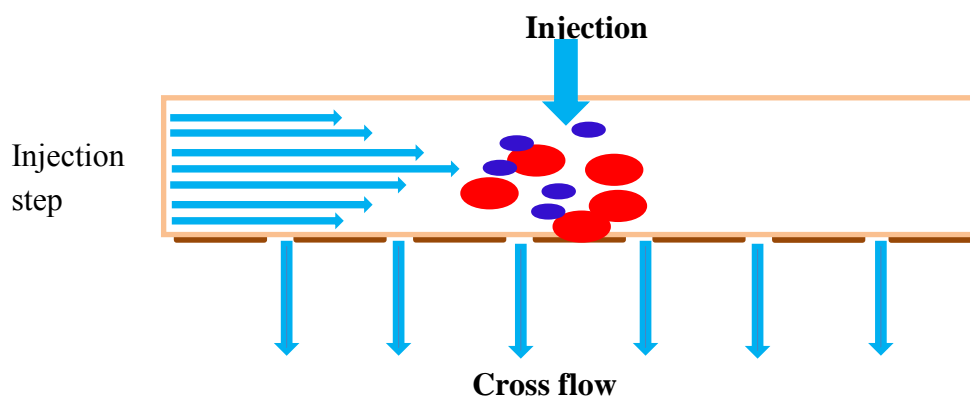


Fig. 2.5a Schematic presentation of the injection step in AF4

Focusing/relaxation step: In the focusing/relaxation step an opposing stream of carrier flow is pumped into the channel from the outlet end in addition to the flow through the inlet port. The step is of high importance since it prevents diffusion in the longitudinal direction minimizing axial band broadening of the sample while it is confined to a position near the inlet port (Fig. 2.5b)^{17,21}. This helps the analytes to be positioned in their steady-state equilibrium levels before being eluted, so as to optimize the fractionation “quality”. Unlike other forms of FFF, the field of force in AF4 cannot be controlled independently of the axial flow^{22,23,29}.

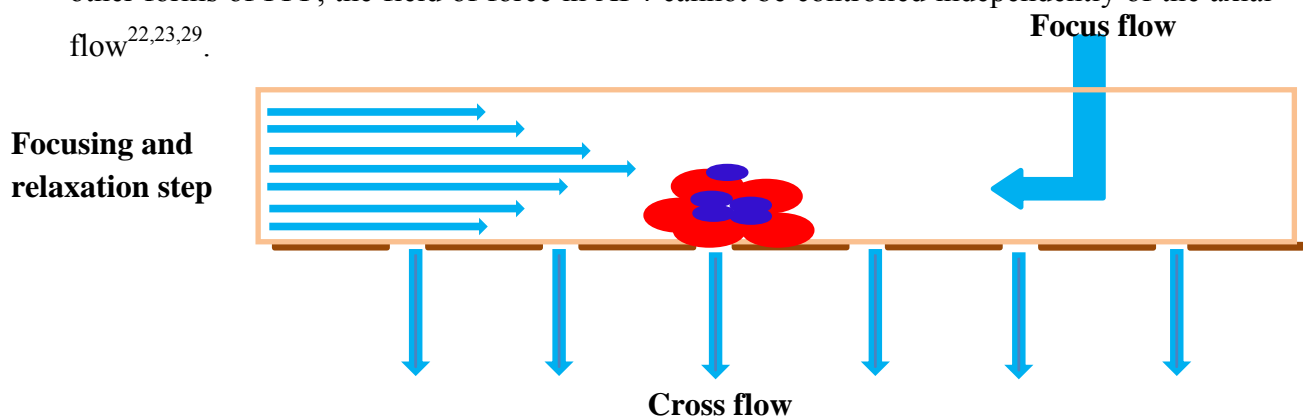


Fig. 2.5b Schematic presentation of the focusing step in AF4

Separation: During the separation process all particles are pushed against the accumulation wall by the cross flow. Due to the ability of the molecules to diffuse and act against this force, the analyte will diffuse back into the channel depending on their diffusion coefficients³². In normal mode the smaller particles will move further away from the accumulation membrane. Macromolecules of different sizes will be situated in different flow layers. The elution time depends on the flow velocity of the respective layer in which the polymer molecules are situated¹⁷.

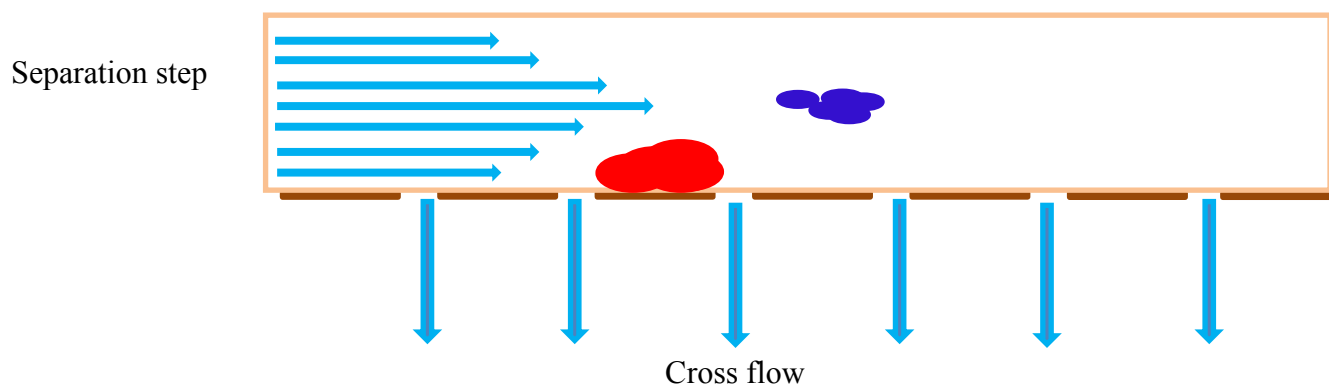


Fig. 2.5c Schematic presentation of the separating step in AF4

2.5 Thermal field-flow fractionation (Thermal FFF)

In Thermal FFF, a temperature gradient is established between two parallel plates (Fig. 2.6 and Fig. 2.7) so as to generate solute migration to one wall (usually the cold one) by thermal diffusion. Thermal diffusion is also called in liquids the Soret effect^{17, 19, 28, 34-38}. Usually heat conducting flat copper plates are used³⁹. To achieve the temperature gradient, the hot wall is kept at an elevated temperature (T_h) through the use of software controlled heating rods and the cold wall is kept cool at lower temperature (T_c) using a recirculating chiller. A temperature drop (ΔT equal to T_h minus T_c) is usually in the range 30–100 K, which results in a strong temperature gradient (up to 104 K/cm in a 100 μm thickness channel). Thermal FFF channels are usually pressurized to 8–10 bar to increase the boiling point of the carrier liquid. In Thermal FFF, the thermal diffusion coefficient (D_T) is a basic transport coefficient describing the movement of matter under an applied temperature gradient and it is generally

independent of the molar mass. The theory of Thermal FFF shows that retention is dependent on the thermal diffusion coefficient D_T which in turn is also dependent on the chemical composition of the polymer and solvent used³⁹⁻⁴¹. The transport of polymers by thermal diffusion usually occurs in the direction of the cold plate⁴⁰.

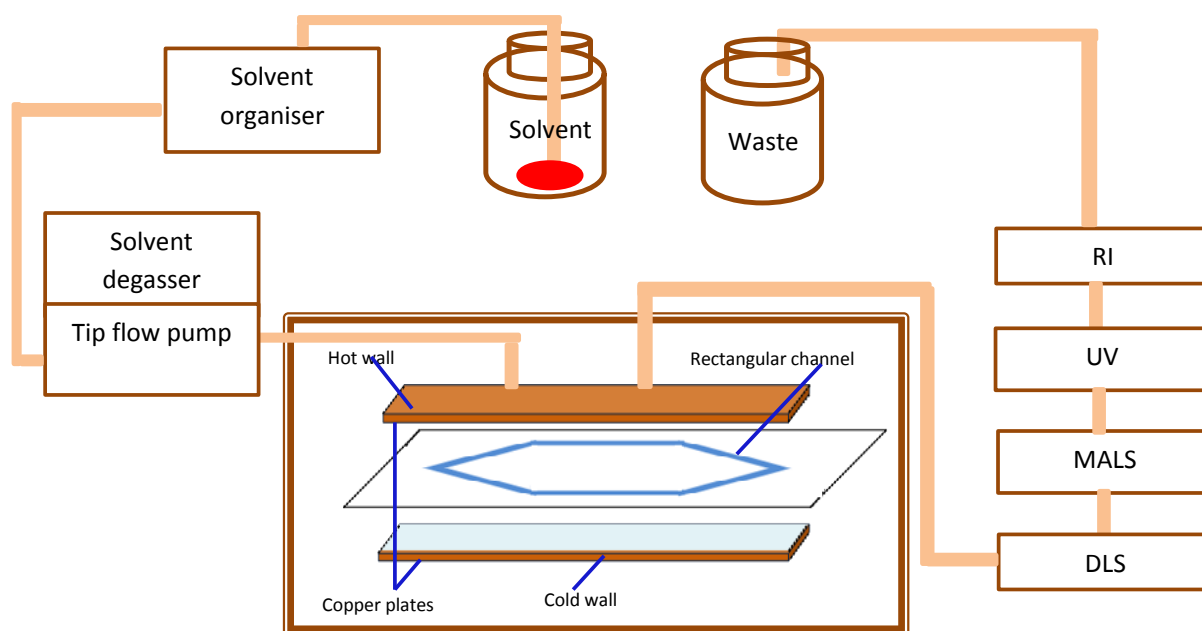


Fig. 2.6 Schematic representation of the Thermal FFF instrumentation setup at Stellenbosch University.

The thermal diffusion (D_T) combined with the magnitude of the ordinary diffusion (D), determines how far a given solute will extend in the fast streamlines of the laminar flow. This in turn, determines the solute average axial velocity. Thermal field-flow fractionation (Thermal FFF) is a useful technique for separating complex polymer mixtures. The unique features of Thermal FFF make it applicable to many polymers that are difficult to characterize by conventional methods²⁸. The technique has been applied both to colloidal particles (those under 1 μm diameter) and micrometer size particles up to 20 μm diameter⁴⁰.

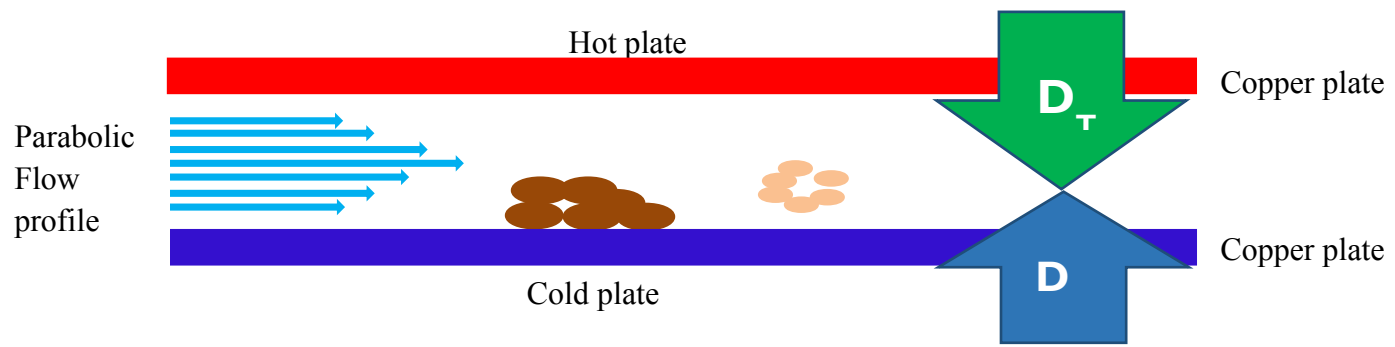


Fig. 2.7 Schematic presentation of Thermal FFF

Assuming the applied temperature gradient is linear across the channel thickness, λ can be represented by Equation 13

$$\lambda = \frac{D}{D_T \Delta T} \quad (13)$$

where D is the ordinary diffusion coefficient, ΔT is the temperature difference applied across the channel thickness assuming a constant gradient. D_T (thermal diffusion coefficient) is affected by the chemical composition of the polymer and the carrier liquid. However D_T is independent of the molar mass for many homopolymers. As a result, Thermal FFF can be used to fractionate homopolymers and copolymers according to chemical composition. In Thermal FFF, R can be measured experimentally and related to λ . However, a modified form of Equation 6 must be used to account for the deviation from the parabolic velocity flow profile that arises from changes in carrier liquid viscosity and thermal conductivity across the channel thickness due to the applied ΔT . The modified equation includes a velocity distortion factor term V as shown in Equation 14

$$R = \frac{t^0}{t_r} = 6\lambda \left[v + (1 - 6\lambda v) \left[\coth \frac{1}{2\lambda} - 2\lambda \right] \right] \quad (14)$$

2.6 Applications of AF4 and Thermal FFF

AF4 and Thermal FFF have never been used to analyse PS-b-PEO block copolymers in different single solvents. Only a few amphiphilic block copolymers have been characterized using AF4 and Thermal FFF. Another important amphiphilic block copolymer, Poly(ethyleneoxide-b-caprolactone) (PEO-b-PCL) which self-assembles in water has been characterized using AF4-QELS (quasielastic light scattering)-MALLS-UV³¹. The nanoparticle sizes obtained by AF4 were similar to those obtained by DLS (Dynamic light scattering detector). This proved that AF4 is a suitable technique for size determination of nanoparticles. Ehrhart et al. also obtained several nanoparticles with very different sizes using AF4 only³¹. In our group we recently characterized and fractionated poly(styrene-b-isoprene) (PS-b-PI) diblock copolymers synthesized by either sequential living anionic polymerization or coupling of living precursor blocks using AF4. In this study THF was used as the eluent and AF4 successfully separated the bulk polymer samples into their respective block copolymer fractions, homopolymers and coupling by-products⁴². AF4 was also used to analyse the molar mass of the different components. Separation in AF4 is based on differences in hydrodynamic sizes¹⁷.

In most FFF techniques, retention can be predicted as a function of primary polymer or particle properties such as mass, density, hydrodynamic diameter, diffusivity, charge and so on³⁹. However in Thermal FFF retention is complicated because thermal diffusion can be related to various thermal diffusion parameters such as the Soret coefficient (D_T/D) (which determines the average analyte distance from the accumulation wall), the thermal diffusion factor α , and the thermal diffusion coefficient (D_T) as well as the ordinary diffusion coefficient (D) which also influences retention^{36, 39, 43}. To obtain the thermal diffusion coefficient (D_T), the ordinary diffusion coefficient D has to be known⁴⁴. Thus retention in Thermal FFF can be a result of different molar masses or chemical compositions. Previously, D values have been measured using offline methods. These included the combination of size exclusion chromatography (SEC) and thermal field-flow fractionation (Thermal FFF) with mass and viscosity detectors^{45, 46}. Polymer standards and the universal calibration concept were used to determine the dependence of retention on the diffusion coefficient (D) in the SEC column. Then the polymers were separated in SEC to obtain their respective D values. The D values from SEC and the Thermal FFF retention parameter were then used to calculate

D_T ^{46, 47}. However this required long analysis times and it posed difficulties in finding the optimum separation conditions for each dimension. Other offline methods include the use of dynamic light scattering (DLS)⁴⁸ by batch measurements to determine D from hydrodynamic radii by using the Stokes-Einstein equation⁴⁹. The above mentioned limitations were overcome by online measurements of D and D_T through coupling thermal field-flow fractionation (Thermal FFF) with online multiangle light scattering, differential refractive index and quasielastic light scattering (Thermal FFF-MALLS/dRI/QELS) detectors³⁶. The major advantage of this recently discovered combination was that D values could be measured continuously as the analyte eluted from the Thermal FFF channel. This allowed online measurements of D values to take place thus yielding the chemical composition distribution of the polymers. In this work we also did online measurements of the D values.

The thermal diffusion of macromolecular materials as well as its relationship to physicochemical parameters such as molar mass and hydrodynamic diameter is poorly understood. As a result of this, Thermal FFF has become the most widely used technique for exploring these relationships³⁹. The ability of Thermal FFF to differentially retain macromolecules of the same chemical composition but different size has also been discovered²⁸. In such cases retention has been found to depend not only on molar mass but also on polymer and solvent composition^{39, 44, 47}. However the change in flow rate of the carrier liquid and the temperature profile across the channel at different ΔT also affect retention. When the temperature difference between the hot and cold wall (ΔT) increases the retention time also increases. This also increases the fractionation power at a constant flow rate. On the contrary, an increase in flow rate reduces the analysis time, however, the fractionation power decreases. For higher molar mass polymers an increase in flow rate reduces the tendency of polymers to interact with the channel walls¹⁷.

Interestingly, D_T is independent of the temperature gradient but was found to be strongly affected by the chemical composition of both the polymer and the solvent⁴⁸. In addition to the use of Thermal FFF in understanding thermal diffusion of macromolecules, it has been successfully used in the fractionation and characterization of various lipophilic polymers⁴⁸. These lipophilic homopolymers include polystyrene (PS)^{39, 44, 47, 48, 50-52}, poly(methyl methacrylate) (PMMA)^{40, 47} and polyisoprene (PI)⁴⁷. For homopolymers Thermal FFF separation is based on solute molar mass since D_T remains constant and D decreases with increase in molar mass⁴⁵. D_T values as well as retention ratios have been calculated for these

homopolymers. These D_T values have been found to be independent of the molar mass of the homopolymers but dependent on their chemical composition as well as the solvent used⁴⁸, as mentioned earlier.

There have been very few examples previously published on the behaviour of copolymers because of two main reasons. Firstly, the limited availability of well characterized copolymer standards which vary in molar mass, composition and microstructure has prevented a thorough investigation of D_T as function of these variables^{36, 53}. The second reason was that D values were acquired from external measurements or offline methods which had several limitations, some of which were mentioned above^{36, 47, 48}.

The behaviour of copolymers in Thermal FFF is complex, it depends on the copolymer type as well as solvent used. For random copolymers in both selective and non-selective solvents which were thermodynamically favourable for both monomer components, a linear dependence of D_T on monomer content was found^{36, 48}. A similar linear dependence for PS-*b*-PI-*b*-PS triblock copolymers was observed, D_T increased with the increase of wt% of PS⁴⁵. However for block copolymers in a selective solvent D_T is affected by the monomer units located in the outer region of the polymer molecule. When a non-selective solvent is used D_T follows the same pattern as that in random copolymers^{36, 43, 45, 46}. Jeon et al. used a combination of SEC and Thermal FFF with mass and viscosity detectors to characterize and fractionate blends of polystyrene-polyethylene oxide diblock copolymers (PS-*b*-PEO) and their corresponding homopolymers. They obtained D values from SEC, which were used together with their Thermal FFF retention parameters to calculate D_T values in 5:1 (v/v) THF/DMF. The D_T values were found to be linearly dependent on the copolymer composition⁴⁶. Thermal FFF-MALS/dRI/QELS, was used to determine simultaneously the molar mass and composition of polystyrene-poly(*n*-methyl acrylate) (PS-*b*-PMA) and polystyrene-poly(*n*-butyl acrylate) (PS-*b*-PBA). This allowed the online determination of D values by QELS which were used to calculate the D_T values as the copolymers eluted from the Thermal FFF channel. The copolymer D_T values were found to be independent of the molar masses for copolymers with similar chemical compositions but dependent on composition for copolymers with similar molar masses in a good solvent for both polymer blocks³⁶. However, the FFF behaviour of PS-*b*-PEO copolymers and their respective homopolymers in different single solvents in Thermal FFF and AF4 has not been investigated.

2.7 Detectors

In order to monitor polymers eluting from the separating systems, different detectors are required. The most commonly used detectors are refractive index (RI), viscometric, evaporative light scattering detector (ELSD) and multiangle laser light scattering (MALLS) detectors. When choosing the detector type one must consider both the nature of the sample and the type of information required⁵⁴. RI and UV are the most common concentration sensitive detectors. The RI and UV peak intensities depend on the concentration of the solute molecules in the mobile phase. For a molar mass sensitive detector like MALLS, the peak intensities are proportional to the product of concentration and molar mass.

2.7.1 Refractive index detector (RI)

The use of refractive index detection for dissolved polymers is well known. RI detection for polymer samples that lack an accessible UV/Vis absorption band makes it a universal concentration sensitive detector¹⁷. However the polymers should have a non-zero specific refractive index increment (dn/dc). The dn/dc value is very important for molar mass determinations from light scattering measurements as an error in the dn/dc value will cause a large error equal to $(dn/dc)^2$ in molar mass calculations. The RI response is dependent on both the polymer concentration and chemical composition⁵⁴.

2.7.2 Dynamic light scattering detector (DLS) (zetasizer)

DLS is also known as the quasielastic light scattering or photon correlation spectroscopy. This technique measures the diffusion coefficients of colloidal particles and macromolecules dissolved or dispersed undergoing Brownian motions in a solvent^{30, 54}. It does this by analysing the correlation of the fluctuation of light intensity over time using a mathematical process called autocorrelation^{48, 54}. For a monodispersed polymer standard, the normalized autocorrelation function is given by equation 15

$$g(\tau) = e^{-Dq^2 \tau} \quad (15)$$

where D is the so-called mutual diffusion coefficient, τ is the delay time, and q is the scattering vector that can be considered as an experimental constant [$q = 4\pi \sin(\Theta/2)/\lambda_1$, where Θ is the scattering angle and λ_1 the wavelength of the incident light]. The analysis of the autocorrelation function allows determination of mutual diffusion^{48, 54}. The fluctuations reflect the motion of the scattering particle. Large particles move slowly, the intensity fluctuates slowly too thus resulting in small diffusion coefficient values while for small particles moving rapidly the fluctuations are rapid too. Using the diffusion coefficient from DLS yields information on the hydrodynamic radius (R_h) using the Stokes-Einstein relation⁵⁵

$$R_h = \frac{kT}{6\pi\eta D} \quad (16)$$

where K is Boltzmann's constant, T is the absolute temperature, and η is the solvent viscosity. Online coupling of FFF-DLS allows the determination of hydrodynamic diameters. The fractionation of FFF provides less polydisperse samples hence it improves DLS analysis^{30, 31, 36}. However for Thermal FFF, the diffusion measurements should be performed at a temperature and polymer concentration that match the operating conditions in DLS⁴⁸.

2.7.3 Multiangle light scattering (MALLS)

MALLS is a type of static light scattering. It is an absolute technique for measurements of molar masses⁵⁶. Static light scattering may also be called elastic, Rayleigh, or classical light scattering. MALLS measures average intensity fluctuations while DLS measures the fluctuations of the scattered light intensity⁵⁴. A MALLS detector measures the scattered signal from polymers or particles in a sample at different scattering angles Θ in relation to the incoming light^{54, 57, 58}. The light scattering data obtained from the detector are fitted to different models of which the Debye, Zimm, and Berry models are commonly used. These models allow the determination of the radius of gyration (R_g), from the slope of a curve fitted to the angular dependence of the intensity of scattered light. When the refractive index increment with concentration (dn/dc) is known for the polymer, and a concentration detector

is used, the weight average molar mass (M_w) of each fraction can be determined from the intersection of the fitted curve⁵⁷.

MALLS detectors use an array of detectors positioned around the flow cell to measure the angular dependence of scattering from polymers⁵⁹ eluting from the channel. The most common equation that relates the intensity of scattered light to the properties of the macromolecules is the Debye equation:

$$\frac{R_\theta}{K^*} = MP(\theta) - 2A_2cM^2 P^2(\theta) \quad (17)$$

where R_θ is the Rayleigh ratio, K^* is an optical constant, c is the polymer concentration in solution, M is molar mass $P(\theta)$ is the particle scattering factor (function of angular dependence) and A_2 is the second virial coefficient. The optical constant is given by:

$$K^* = \frac{4\pi^2 n_0^2}{\lambda_0^4 N_A} (dn/dc)^2 \quad (18)$$

Light scattering, in conjunction with concentration detection, allows for direct molar mass determination without calibration against molar mass standards or by assumptions regarding scaling between mass and size. Thus, it is a powerful tool for the characterization of samples fractionated by AF4^{30, 54, 56, 57, 59-61}.

2.8 References

1. Malik, M. I.; Harding, G. W.; Grabowsky, M. E.; Pasch, H. *J. Chromatogr. A* **2012**, 1244, 77–87.
2. Zushun, X.; Linxian, F.; Jian, J.; Shiyuan, C.; Yongchun, C.; Changfeng, Y. *Elsevier Science* **1998**, 34, (10), 1499–1504.
3. Lou, X.; van Dongen, J. L. J.; Meijer, E. W. *J. Chromatogr. A* **2012**, 1237, 72–79.
4. Luo, C.; Han, X.; Gao, Y.; Liu, H.; Hu, Y. *J. Dispersion Sci. Technol.* **2011**, 32, (2), 159–166.
5. Ahmad, F.; Baloch, M. K.; Jamil, M.; Jeon, Y. J. *J. Appl. Polym. Sci.* **2009**, 118, (3), 1704–1712.
6. Topel, Ö.; Çakir, B. A.; Budama, L.; Hoda, N. *J. Mol. Liq.* **2013**, 177, 40–43.
7. Caldérara, F.; Hruska, Z.; Hurtrez, G.; Lerch, J. P.; Nugay, T.; Riess, G. *Macromolecules* **1994**, 27, (5), 1210–1215.
8. Bhargava, P. Self-assembled polystyrene-block-poly (ethylene oxide) (PS-b-PEO) micelle morphologies in solution. University of Akron, 2007.
9. Mass, V.; Bellas, V.; Pasch, H. *Macromol. Chem. Phys.* **2008**, 209, (19), 2026–2039.
10. Sinha, P.; Hiller, W.; Bellas, V.; Pasch, H. *J. Sep. Sci.* **2012**, 35, (14), 1731–1740.
11. Sinha, P.; Grabowsky, M.; Malik, M. I.; Harding, G. W.; Pasch, H. *Macromol. Symp.* **2012**, 313–314, (1), 162–169.
12. Malik, M. I.; Sinha, P.; Bayley, G. M.; Mallon, P. E.; Pasch, H. *Macromol. Chem. Phys.* **2011**, 212, (12), 1221–1228.
13. Guzonas, D. A.; Boils, D.; Tripp, C. P.; Hair, M. L. *Macromolecules* **1992**, 25, (9), 2434–2441.
14. Giddings, J. C. *J. Sep. Sci.* **1966**, 123–125, (1).
15. Kowalkowski, T.; Buszewski, B.; Cantado, C.; Dondi, F. *Crit. Rev. Anal. Chem.* **2006**, 36, (2), 129–135.
16. Giddings, J. C.; Yang, F. J.; Myers, M. N. *J. Virol.* **1977**, 21, (1), 131–138.
17. Schimpf, M. E.; Caldwell, K.; Giddings, J. C., *Field-Flow Fractionation Handbook*. Jonh Wiley and Sons: New york, 2000.
18. Litzen, A.; Wahlund, K.-G. *Anal. Chem.* **1991**, 19, 1001–1007.
19. Messaud, F. A.; Sanderson, R. D.; Runyon, J. R.; Otte, T.; Pasch, H.; Williams, K. S. *R. Prog. Polym. Sci.* **2009**, 34, 351–368.

20. Runyon, J. R.; Goering, A.; Yong, K.-T.; Williams, S. K. R. *Anal. Chem.* **2013**, *85*, (2), 940–948.
21. Roda, B.; Zattoni, A.; Reschiglian, P.; Moon, M. H.; Mirasoli, M.; Michelini, E.; Roda, A. *Anal. Chim. Acta.* **2009**, *635*, (2), 132–143.
22. Fraunhofer, W.; Winter, G. *European journal of pharmaceuticals and biopharmaceutics : official journal of Arbeitsgemeinschaft fur Pharmazeutische Verfahrenstechnik e.V* **2004**, *58*, (2), 369–383.
23. Fraunhofer, W. Asymmetrical flow field-flow-fractionation in pharmaceutical analytics. University of München, 2003.
24. Yohannes, G.; Wiedmer, S. K.; Elomaa, M.; Jussila, M.; Aseyev, V.; Riekkola, M.-L. *Anal. Chim. Acta* **2010**, *675*, (2), 191–198.
25. Gimbert, L. J.; Andrew, K. N.; Haygarth, P. M.; Worsfold, P. J. *Trends Anal. Chem.* **2003**, *22*, (9), 615–633.
26. Otte, T.; Brüll, R.; Macko, T.; Pasch, H.; Klein, T. *J. Chromatogr., A* **2010**, *1217*, (5), 722–730.
27. Prestel, H.; Schott, L.; Niessner, R.; Panne, U. *Water Res.* **2005**, *39*, (15), 3541–3552.
28. Schimpf, M. E. *J. Chromatogr.* **1990**, *517*, 405–421.
29. Reschiglian, P.; Zattoni, A.; Roda, B.; Michelini, E.; Roda, A. *Trends Biotechnol.* **2005**, *23*, (9), 475–483.
30. Baalousha, M.; Stolpe, B.; Lead, J. R. *J. Chromatogr., A* **2011**, *1218*, 4078–4103.
31. Ehrhart, J.; Mingotaud, A. F.; Violleau, F. *J. Chromatogr., A* **2011**, *1218*, 4249–4256
32. Wittgren, B.; Wahlund, K.-G. *J. Chromatogr., A* **1997**, *791*, 135–149.
33. Wijnhoven, J. E. G. J.; Bommel, v. M. R.; Poppe, H.; Kok, W. T. *Chromatographia* **1996**, *42*, 409–415.
34. Kassalainen, G. E.; Williams, S. K. R. *Anal. Chem.* **2003**, *75*, (8), 1887–1894.
35. Williams, S. K. R.; Shiundu, P. M.; Calvin Giddings, J. *Colloids Surf., A* **1995**, *105*, 243–250.
36. Runyon, J. R.; Williams, S. K. R. *J. Chromatogr., A* **2011**, *1218*, (38), 6774–6779.
37. Shiundu, P. M.; Munguti, S. M.; Williams, S. K. *J. Chromatogr., A* **2003**, *983*, 163–176.
38. Williams, S. K. R.; Runyon, J. R.; Ashames, A. A. *Anal. Chem.* *83*, (3), 634–642.
39. Sisson, R. M.; Giddings, J. C. *Anal. Chem.* **1994**, *66*, (22), 4043–4053.
40. Martin, M.; Reynaud, R. *Anal. Chem.* **1980**, *52*, (14), 2293–2298.
41. Shiundu, P. M.; Calvin Giddings, J. *J. Chromatogr., A* **1995**, *715*, (1), 117–126.

42. Makan, A.; Sinha, P.; Ngaza, N.; Aswegen, W.; Pasch, H. *Anal. Bioanal. Chem.* **2013**, 1–7.
43. Runyon, J. R.; Williams, S. K. *J. Chromatogr.* **2011**, 1218, (39), 6774–6779.
44. Giddings, J. C.; Caldwell, K. D.; Myers, M. N. *Macromolecules* **1976**, 9, (1), 106–112.
45. Cho, K.-H.; Park, Y. H.; Jeon, S. J.; Kim, W.-S.; Lee, D. W. *J. Liq. Chromatogr. Relat. Technol.* **1997**, 20, (16–17), 2741–2756.
46. Jeon Sun, J.; Schimpf Martin, E., Cross-Fractionation of Copolymers Using SEC and Thermal FFF for Determination of Molecular Weight and Composition. In *Chromatography of Polymers*, American Chemical Society: 1999; Vol. 731, pp 141–161.
47. Gunderson, J. J.; Giddings, J. C. *Macromolecules* **1986**, 19, (10), 2618–2621.
48. Van Asten, A. C.; Kok, W. T.; Tijssen, R.; Poppe, H. *J. Polym. Sci., Part B: Polym. Phys.* **1996**, 34, (2), 283–295.
49. Mes, E. P. C.; Tijssen, R.; Kok, W. T. *J. Chromatogr., A* **2001**, 907, 201–209.
50. Myers, M. N.; Cao, W.; Chen, C.-I.; Kumar, V.; Giddings, J. C. *J. Liq. Chromatogr. Relat. Technol.* **1997**, 20, (16–17), 2757–2775.
51. Rue, C. A.; Schimpf, M. E. *Anal. Chem.* **1994**, 66, (22), 4054–4062.
52. Kassalainen, G. E.; Williams, S. K. R. *J. Chromatogr., A* **2003**, 988, (2), 285–295.
53. Batten, C.; Hoyos, M.; Martin, M. *Chromatographia* **1997**, 45, (1), 121–126.
54. Podzimek, S., Polymers. In *Light Scattering, Size Exclusion Chromatography and Asymmetric Flow Field Flow Fractionation*, John Wiley & Sons, Inc.: 2011
55. Lattuada, M.; Olivo, C.; Gauer, C.; Storti, G.; Morbidelli, M. *Langmuir* **2010**, 26, (10), 7062–7071.
56. Wittgren, B.; Wahlund, K.-G. *J. Chromatogr., A* **1997**, 760, (2), 205–218.
57. Nilsson, L. *Food Hydrocolloids* **2013**, 30, (1), 1–11.
58. Mes, E. P. C.; de Jonge, H.; Klein, T.; Welz, R. R.; Gillespie, D. T. *J. Chromatogr., A* **2007**, 1154, 319–330.
59. White, R. J. *Polym. Int.* **1997**, 43, (4), 373–379.
60. Roessner, D.; Kulicke, W.-M. *Anal. Chem.* **1995**, 67, (18), 3229–3233.
61. Gigault, J.; Grassl, B.; Lespes, G. T. *Chemosphere* **2012**, 86, (2), 177–182.

Chapter 3:

Experimental

3.1 Chemicals

3.1.1 Solvents used for thermal field-flow fractionation (Thermal FFF)

- Tetrahydrofuran (THF, HPLC grade) obtained from Sigma-Aldrich (Sigma-Aldrich, South Africa)
- Toluene, HPLC grade (Sigma-Aldrich, South Africa)
- Chloroform, HPLC grade (Sigma-Aldrich, South Africa)

3.1.2 Solvents used for asymmetrical flow field-flow fractionation (AF4)

- Acetonitrile (ACN), HPLC grade (Sigma-Aldrich, South Africa)
- Chloroform, HPLC grade (Sigma-Aldrich, South Africa)

3.1.3 Polymer standards

Polystyrene (PS) calibration standards from Polymer Laboratories (PL) (Polymer Laboratories, Church Stretton, Shropshire, UK) were used. These covered a range of different molar masses. Polyethylene oxide (PEO) standards were products of Polymer Standards Service GmbH (Mainz, Germany).

Table 3.1 PS and PEO calibration standards

PS M_p(g/mol)	PEO M_p(g/mol)
29 500	44 300
132 000	81 900
275 000	289 000
1 412 000	1 015 000

3.1.4 Copolymers

The PS-b-PEO copolymers were from PSS (Polymer Standards Service GmbH, Mainz, Germany) and the sample details from the supplier are as follows:

Table 3.2 PS-b-PEO block copolymer details according to the manufacturer

PS-b-PEO	M _w total (g/mol)	M _w PS (g/mol)	M _w PEO (g/mol)
1	5 460	1 500	3 960
2	31 930	2 930	29 000
3	91 500	30 000	61 500
4	218 000	109 000	109 000
5	2 280 000	1 200 000	1 080 000

3.2 Field-flow fractionation techniques

3.2.1 Thermal field-flow fractionation (Thermal FFF) system

All Thermal FFF measurements were performed using a Thermal FFF system TF2000 from Postnova (Landsberg, Germany) which was coupled to a MALLS (PN3070) detector from Postnova Analytics (Landsberg/Germany), zetasizer ‘Zetasizernano’ series S173 (PN3704) detector from Postnova Analytics (Landsberg/Germany), UV detector from Postnova Analytics (Landsberg/Germany) and RI (PN 3140) detector from Postnova Analytics (Landsberg/Germany). The Thermal FFF channel was connected to a solvent organizer, degasser and a pump. The Mylar spacer used for definition of the channel height had a thickness of 350 µm.

Suitable backpressure tubing was connected between the channel and the first detector tubing in order to prevent the organic solvent from boiling at temperatures above their boiling points

on the hot wall. This helped to increase the system pressure to a level higher than the solvent vapor pressures at the given hot wall temperature.

Temperature calibrations for the different solvents were conducted in order to monitor and configure the temperature control system. This was done automatically on the heater window using the TF2000 software. The temperature calibrations were important for the system to drive temperature conditions corresponding to the programmed method.

3.2.2 Asymmetrical flow field-flow fractionation (AF4) system

All AF4 measurements were performed using an ambient temperature AF4-Instrument from Postnova Analytics (Landsberg/Germany) which was coupled to a MALLS (Dawn DSP) detector from Wyatt Technology (Santa Barbara/USA) and a RI-detector (PN 3140) from Postnova Analytics (Landsberg/Germany). The AF4 channel was connected to three different pumps (tip, focus and cross-flow). A regenerated cellulose membrane was used for the AF4 channel with an average cut-off molar mass of 10 kg/mol. The Mylar spacer used for definition of the channel height had a thickness of 350 μm .

3.3 Calibration of the RI and MALLS detectors with PS calibration standards in THF

3.3.1 Calibration of the RI detector

The RI detector was calibrated first using a PS 62KDa calibration standard as isotropic scatterer in THF with a concentration of 2 mg/ml and a dn/dc value of 0.185 ml/g. For calibration of the RI detector, a run without focusing and a temperature gradient was used. The RI detector was calibrated so as to obtain accurate concentration values for the polymers.

3.3.2 Calibration of the MALLS detector

The calibration procedure for the MALLS detector was divided into two steps. The first part was the calibration of the 90 ° angle. The MALLS detector was also calibrated in THF with a PS 62KDa calibration standard as isotropic scatterer, which had a concentration of 2 mg/ml and a dn/dc value of 0.185 ml/g. A constant ΔT at 90 °C and a flow rate of 0.3 ml/min was used to separate all possible impurities or water from PS 62KDa to make sure that the detector sees only the calibration standard. After the calibration procedure the 90 ° angle had a correct constant, however, this constant was not valid for all other angles.

The second part was the normalization procedure. In the normalization procedure the constants for all the other angles except the 90 ° angle were calculated using the TF2000 software.

3.4. FTIR-ATR

The reflectance FTIR analysis was carried out on a Thermo Scientific Nicolet iN10 FTIR microscope (Waltham, MA, USA) using the Omnic 8.1.10 with an attenuated total reflectance (ATR) accessory. The PS 132KDa and PEO 81.9KDa homopolymer standards were analysed by FTIR-ATR in powder form. All fractions of selected samples dissolved in their respective solvents were left for several hours to dry. This was followed by a final drying session in the vacuum oven over night at room temperature before any spectra were collected. Several spectra for each sample spot were collected and processed for interpretation.

Chapter 4:

Results and discussion

4.1 Introduction

Up to now only a few amphiphilic block copolymers have been characterized using AF4 and Thermal FFF¹. However, Thermal FFF has been successfully used to characterize various lipophilic polymers with regard to their size as well as chemical composition²⁻⁶. Polymer retention in Thermal FFF is influenced by molar mass and chemical composition. Therefore, Thermal FFF is an interesting tool for investigating the molecular heterogeneity of complex polymers as an alternative to column-based chromatography^{3,7,8}.

In our study Thermal FFF-DLS-MALLS-UV-RI was used to characterize the FFF behaviour of PS-*b*-PEO copolymers, PS and PEO homopolymers, as well as to determine their molar mass and chemical composition distributions in different organic solvents. In Thermal FFF, the retention of polymers is determined by the magnitudes of thermal diffusion coefficient (D_T) and normal diffusion coefficient (D)⁹. The major advantage of the above utilized detector combination was that D values were measured continuously as the analytes eluted from the Thermal FFF channel. The D values were then used to calculate polymer D_T values. For the characterization of the polymers, non-selective (good solvents for both blocks) and selective solvents (good solvent for one block and poor solvent for the other block) for PS were used. Methods with suitable temperature programs and flow rates were to be developed for analysis. Fractions were to be taken and the chemical composition of the fractions was to be determined by Fourier-transform infrared (FTIR) spectroscopy. AF4-MALLS-RI was also utilized in order to characterize the FFF behaviour of PS-*b*-PEO copolymers, PS and PEO homopolymers as well as to determine their molar masses in chloroform. In AF4 polymers are separated as a result of differences in hydrodynamic sizes.

4.2 Thermal FFF fractionations in chloroform

4.2.1 Experimental conditions

The polymer samples were introduced into the channel by manual injection with a flow rate of 0.2 ml/min for 60 seconds. A low inlet flow rate of 0.2 ml/min was used to increase the fractionating power. The focus time utilized was 1 minute and a reverse programmed temperature gradient shown in Fig. 4.1 was utilized. An initial temperature difference

between the hot wall and the cold wall of 40 °C was used, which decreased with time to a final temperature difference of 0 °C. The cold wall temperature (T_C) varied between 23 °C and 26 °C. This method was used because upon trying all possible temperature programs it gave the best resolution for molar masses above 200kDa. In order to calculate D_T values a constant temperature programme has to be used so as to maintain a uniform temperature profile throughout the channel. However, in this section no D_T values were calculated for the polymer samples as a result of the utilized temperature programme.

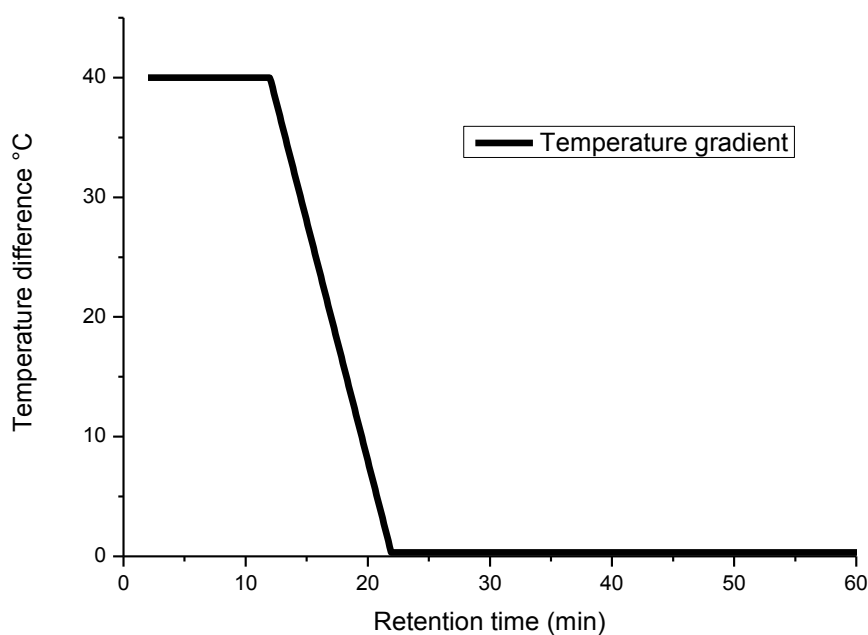


Fig. 4.1 Programmed temperature gradient with T_C 25 °C for polymer analysis.

In this work, chloroform, a good solvent for both PS and PEO was used to characterize the FFF behaviour of the PS-b-PEO copolymers. The FFF behaviour and separation of the PS and PEO homopolymers (see Table 3.1) were also investigated. In chloroform PS as well as PEO homopolymers and PS-b-PEO copolymers dissolve readily, unlike in THF and toluene. The samples were manually injected directly into the Thermal FFF channel at a concentration of 4 mg/ml. No reliable dn/dc for PEO for the solvents utilized in this work were found in literature or determined experimentally. The dn/dc of PEO was estimated from its value in one solvent and difference of the refractive indices of given solvent and the solvent for which the dn/dc is to be estimated. In chloroform, the dn/dc of PEO was estimated from its value in methanol and differences of the refractive indices of methanol and chloroform¹⁰. The dn/dc values of the block copolymers were calculated using the following equation 19:

$$\frac{dn}{dc} = w_{PEO} \left(\frac{dn}{dc}_{PEO \text{ in chloroform}} \right) + w_{PS} \left(\frac{dn}{dc}_{PS \text{ in chloroform}} \right) \quad (19)$$

where w is the weight fraction of PEO or PS in the block copolymers¹⁰ (see Table 3.2). The corresponding calculated dn/dc values of the block copolymers are shown in Table 4.1.

Table 4.1 dn/dc values for PS-b-PEO copolymers, PEO and PS homopolymers calculated for chloroform

Sample name	dn/dc
PS 132kDa	0.14
PS 275kDa	0.14
PS 1412kDa	0.14
PEO 81.9kDa	0.027
PEO 289kDa	0.027
PEO 1015kDa	0.027
PS-b-PEO 218kDa (F1)	0.14
PS-b-PEO 218kDa (F2 bulk polymer sample)	0.084
PS-b-PEO 2280kDa	0.079

4.2.2 Fractionation of PS and PEO homopolymers by Thermal FFF

The fractograms showing the RI and MALLS signals and the molar masses of the PS homopolymers are shown in Figs. 4.2a and b, respectively. An increase in retention time with increase in nominal molar mass can clearly be seen. This is in agreement with the normal mode of separation of the Thermal FFF separation mechanism⁷. Therefore, PS homopolymers were separated according to their molar masses. The utilized temperature program allowed the analysis of PS homopolymers with molar masses that span over a broad molar mass range in a single experiment within a short period of time. The calculated molar mass values obtained from Thermal FFF were close to the nominal values, see Table 4.2.

Table 4.2 Thermal FFF calculated molar masses for PS homopolymers fractionated in chloroform

Sample name	M_w (g/mol)	M_n (g/mol)
PS 132kDa	139 400	122 900
PS 275kDa	223 000	194 200
PS 1412kDa	1 319 000	1 311 000

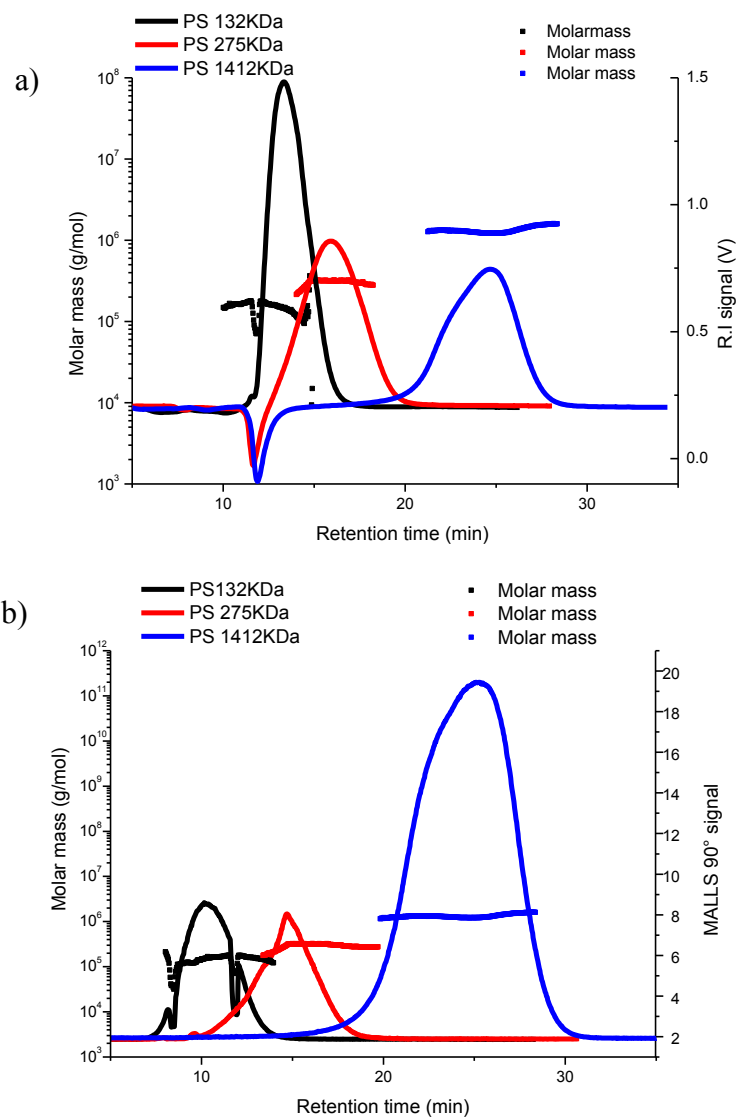


Fig. 4.2 Thermal FFF fractograms in chloroform using a programmed temperature gradient (a) RI signal with molar mass overlaid and (b) MALLS 90° signal with molar mass overlaid. Samples PS 132 kDa, PS 275 kDa and PS 1412 kDa.

Under similar conditions, the PEO homopolymers were fractionated, see the fractograms in Figs. 4.3a and b.

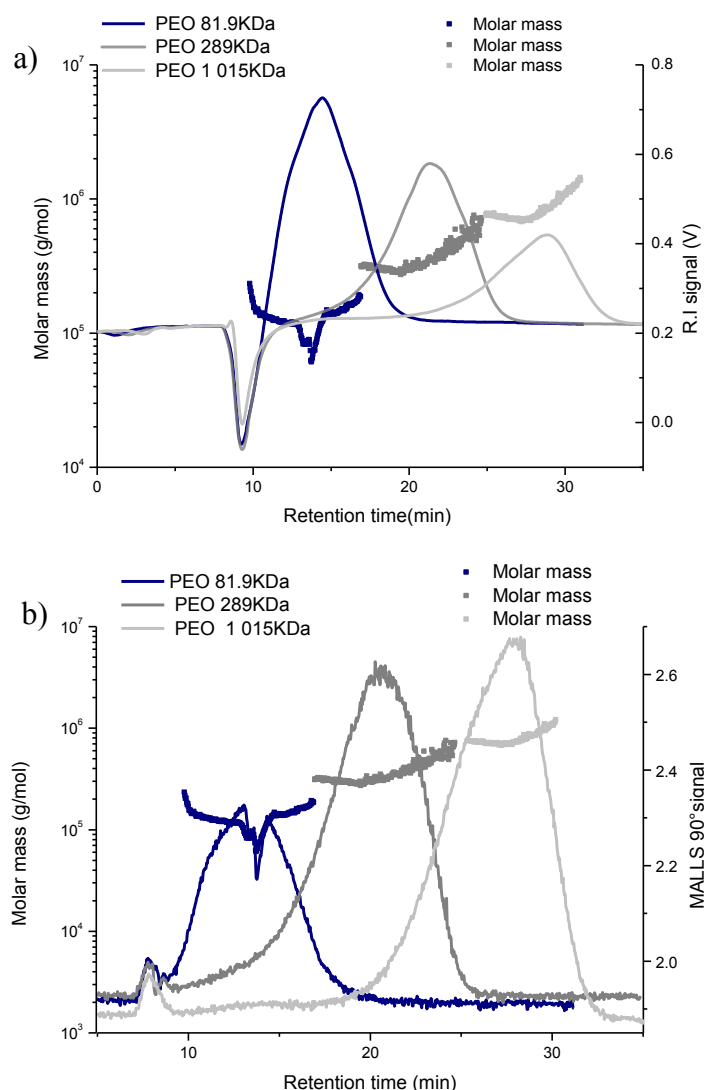


Fig. 4.3 Thermal FFF fractograms in chloroform using a programmed temperature gradient (a) RI signal with molar mass overlaid and (b) MALLS 90° signal with molar mass overlaid. Samples PEO 81.9 kDa, PEO 289 kDa and PEO 1015 kDa.

Similar to the PS homopolymers, the samples eluted in the direction of increasing nominal molar masses. This indicated that the normal FFF fractionation mechanism is prevalent. The molar mass calculated from the MALLS 90° detector signal confirm this separation, however, the agreement with the nominal molar masses is less perfect as compared to PS, see Table 4.3. This could indicate that the PEO molecules do not form extended coil conformations when dissolved in chloroform. Comparing with the work shown later, the calculated molar

mass values in Thermal FFF were closer to the nominal values as compared to AF4, where the homopolymers strongly adsorbed on the cellulose membrane. This led to huge errors in the calculated molar masses which will be shown later for AF4.

Table 4.3 Thermal FFF calculated molar masses for PEO homopolymers fractionated in chloroform

Sample name	M_w (g/mol)	M_n (g/mol)
PEO 81.9kDa	120 300	114 000
PEO 289kDa	344 900	334 000
PEO 1015kDa	800 200	781 200

4.2.3 Fractionation of PS-b-PEO copolymers by Thermal FFF and comparison with PS and PEO homopolymers.

In order to understand the FFF behaviour of PS-b-PEO copolymers in chloroform, these samples were fractionated. Their fractograms were compared to those of PEO and PS homopolymers with molar masses close to the individual blocks in the block copolymers. The fractograms in Figs. 4.4a and b show the RI and MALLS peaks for PS 132kDa, PS-b-PEO 218kDa copolymer and PEO 81.9kDa. It is obvious that in the present case fractionation does not occur strictly according to the total molar mass. The block copolymer has the highest molar mass as confirmed by the MALLS molar mass reading. PEO 81.9kDa has the lowest molar mass but elutes last. PS 132kDa has a significantly lower molar mass than the block copolymer, it co-elutes, however, with the block copolymer. The present results confirm that the fractionation in Thermal FFF is not governed mainly by the normal diffusion coefficient (D) but by the thermal diffusion coefficient (D_T), which is a function of the chemical composition. The influence of the thermal diffusion coefficient (D_T) explains why PS and PEO homopolymers of similar molar masses elute at different retention times, compare e.g. PS 275kDa and PEO 289kDa in Figs. 4.2 and 4.3.

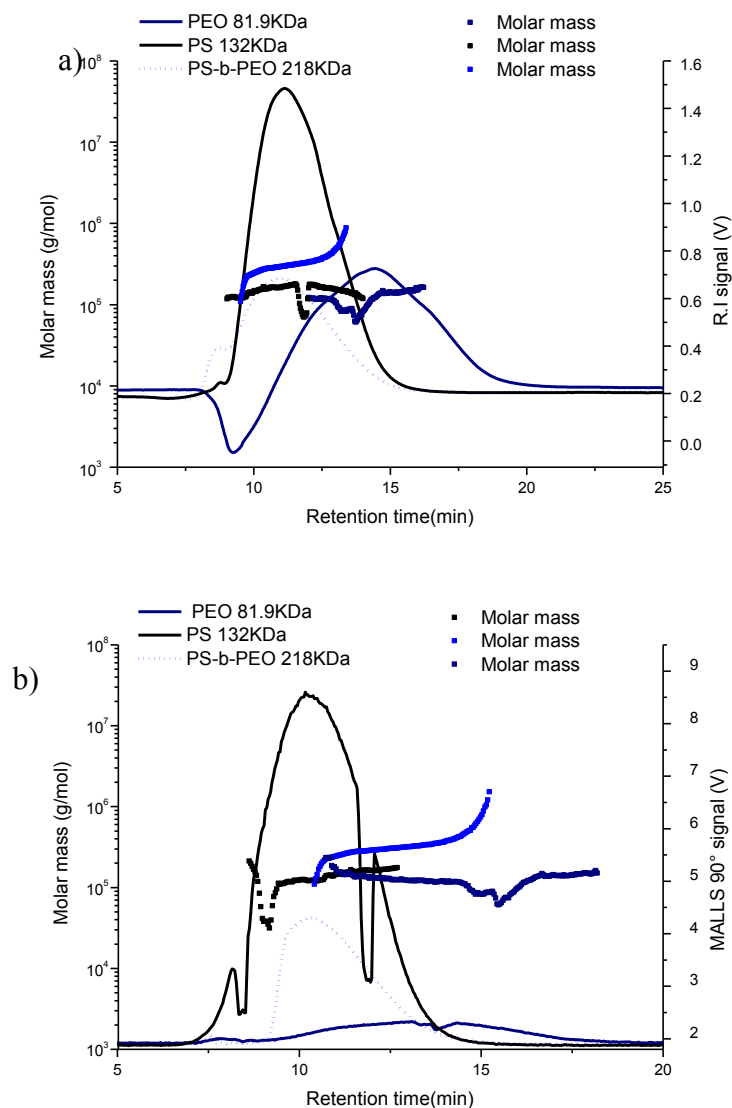


Fig. 4.4 Thermal FFF fractograms in chloroform, (a) RI signal with molar mass overlaid and (b) MALLS 90° signal with molar mass overlaid. Samples PEO 81.9 kDa, PS 132 kDa and PS-b-PEO 218 kDa.

The major influence of the chemical composition on fractionation in Thermal FFF is demonstrated clearly for samples that have similar molar masses, see Fig. 4.5 for PS 275 kDa, PEO 289 kDa and PS-b-PEO 218 kDa. Although they have similar molar masses, no co-elution occurred. The fact that the samples have similar molar masses is proven by the molar mass reading obtained by MALLS.

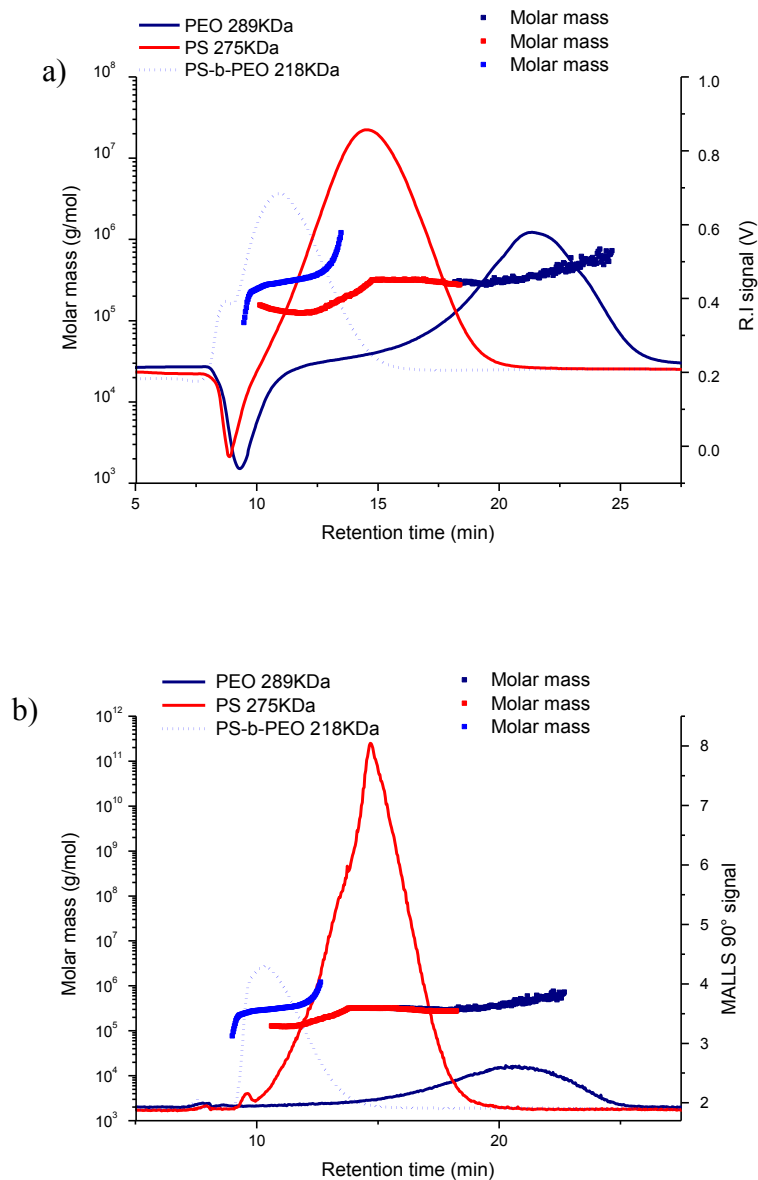


Fig. 4.5 Thermal FFF fractograms in chloroform, (a) RI signal with molar mass overlaid and (b) MALLS 90° signal with molar mass overlaid. Samples PEO 289 kDa, PS 275 kDa and PS-b-PEO 218 kDa copolymer.

As can be seen in Fig. 4.5b, the fractogram of the block copolymer shows some bimodality. In order to obtain more information on the chemical composition as a function of retention time, the PS-b-PEO 218 kDa copolymer was separated into two main sample fractions (denoted F1 and F2) as shown in Figs. 4.6a and b.

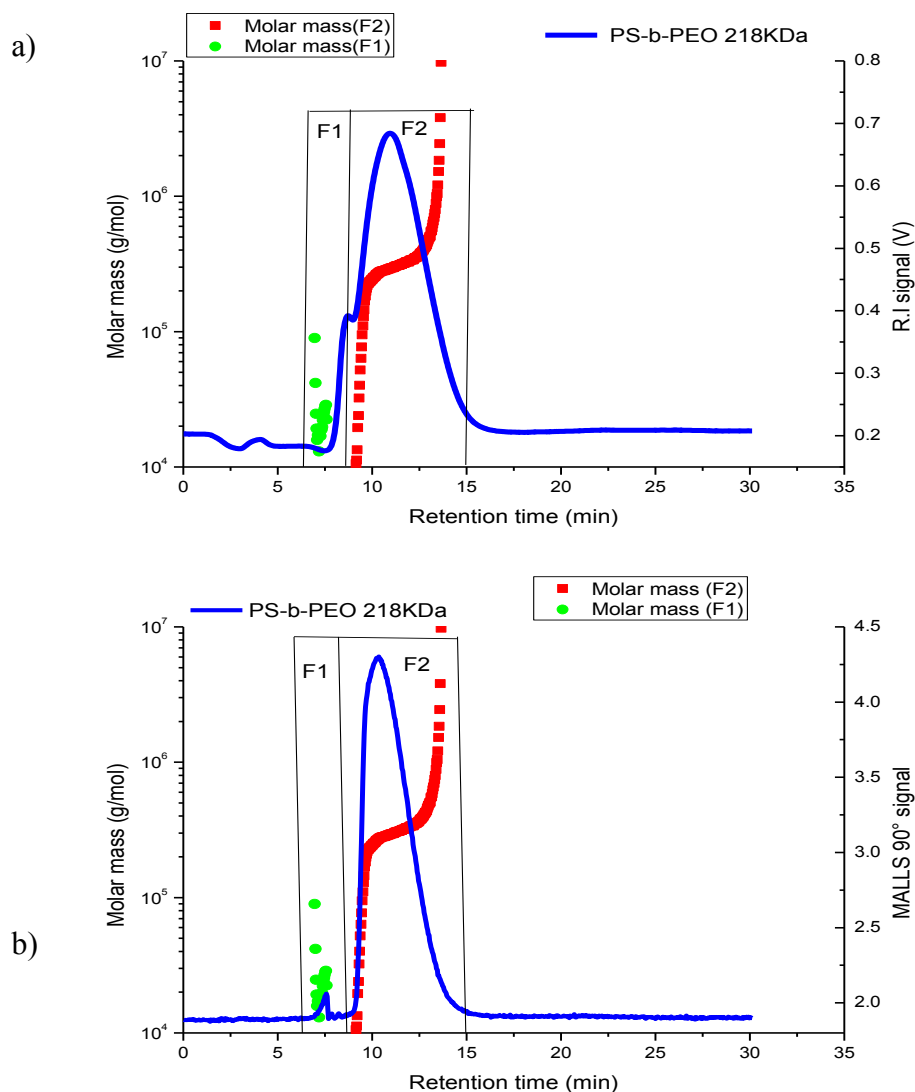


Fig. 4.6 Thermal FFF fractograms in chloroform. (a) RI signal with molar mass overlaid and (b) MALLS 90° signal with molar mass overlaid. Samples PS-b-PEO 218 kDa copolymer (F1 and F2).

The first fraction obtained was labelled F1 and the second F2. From the fractogram, it can be seen that F1 had a significantly lower molar mass than F2 as is indicated in Table 4.4. This shows the normal mode of separation of the Thermal FFF experiment^{7, 8, 18}.

Table 4.4 Thermal FFF calculated molar masses for PS-b-PEO copolymers analysed in chloroform

Sample name	M_w (g/mol)	M_n (g/mol)
PS-b-PEO 218 kDa	30 180	11 890

(F1)		
PS-b-PEO 218 kDa (F2 bulk polymer sample)	234 100	119 700
PS-b-PEO 2280 kDa	2 515 000	2 467 000

In a similar comparison, PS 1412 kDa, PEO 1015 kDa and PS-b-PEO 2280 kDa copolymer were analysed. The block copolymer elutes at slightly different elution times from the homopolymers as shown by the fractograms in Figs 4.7a and b. The components show peak maxima at 21.8, 26.2 and 27.7 minutes for the block copolymer, PS and PEO, respectively. An interesting observation is that PEO 1015 kDa elutes later than PS 1412 kDa and PS-b-PEO 2280 kDa copolymer which have higher molar masses. The elution order is not in agreement with the Thermal FFF normal mode of separation that would suggest separation according to molar mass. The same elution order was also found in Figs 4.4a and b, confirming that the separation is a result of differences in chemical composition.

In Thermal FFF retention is dependent on both molar mass and chemical composition. Therefore FTIR spectroscopy was utilized to obtain information on the chemical composition of the separated components.

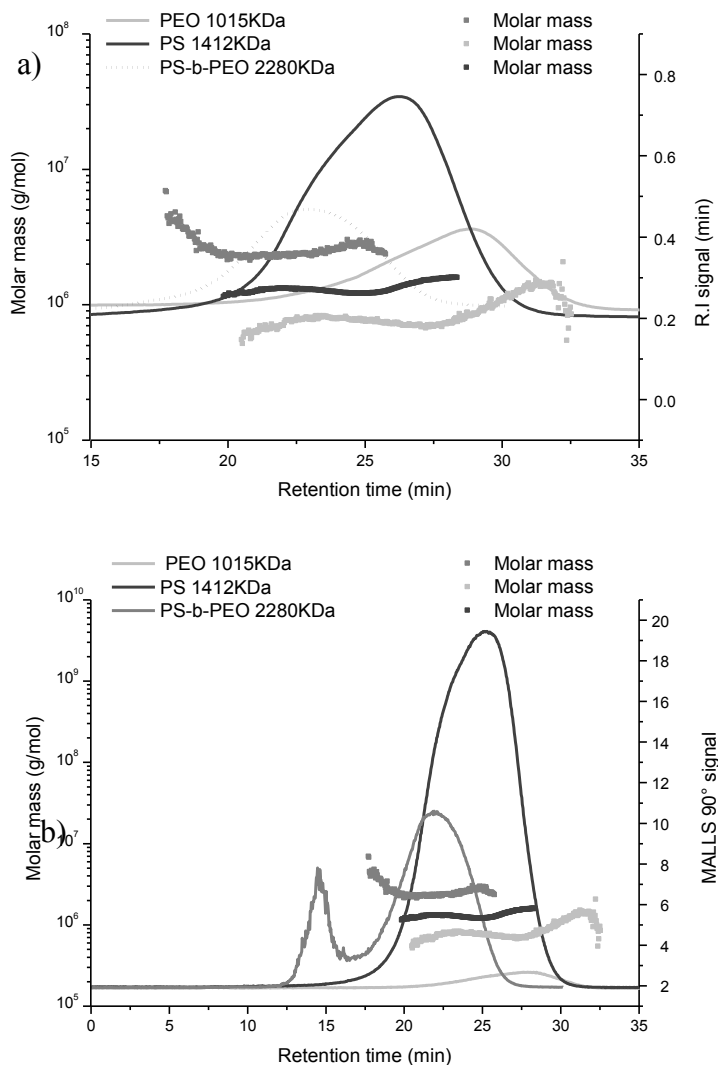


Fig. 4.7 Thermal FFF fractograms in chloroform. (a) RI signal with molar mass overlaid and (b) MALLS 90° signal with molar mass overlaid. Samples PEO 1015 kDa, PS 1412 kDa and PS-b-PEO 2280 kDa copolymer.

4.2.4 Qualitative FTIR analysis of the separated components of PS-b-PEO 218 kDa block copolymer

The polymeric structures of the PS-b-PEO 218 kDa copolymer separated by Thermal FFF in chloroform were collected and then further analyzed by FTIR spectroscopy. The FTIR spectra of the separated components of PS-b-PEO 218 kDa copolymer are shown in Figs.

4.8b and c. The FTIR spectrum of the first polymeric structure F1 (Fig. 4.8c) shows main peaks similar to those for PS (see Fig. 4.8a) at wavenumbers of approximately 700 cm^{-1} (aromatic C-H bend) and 3025 cm^{-1} (aromatic C-H stretch) for PS (red rectangles). Therefore, F1 can be assigned as PS homopolymer. The peaks at wavenumbers of $2880\text{--}3000\text{ cm}^{-1}$ (C-H stretch), $3300\text{--}3600\text{ cm}^{-1}$ (O-H stretch) as well as the range of $840\text{--}1360\text{ cm}^{-1}$ (C-O-C stretch) were assigned to PEO. These peaks are highlighted by purple circles in Figs. 4.8b and d. The FTIR spectrum of the second polymeric structure F2 (Fig. 4.8b) shows co-existing peaks for both PS and PEO, therefore F2 shown in Fig. 4.8b can be assigned PS-b-PEO copolymer.

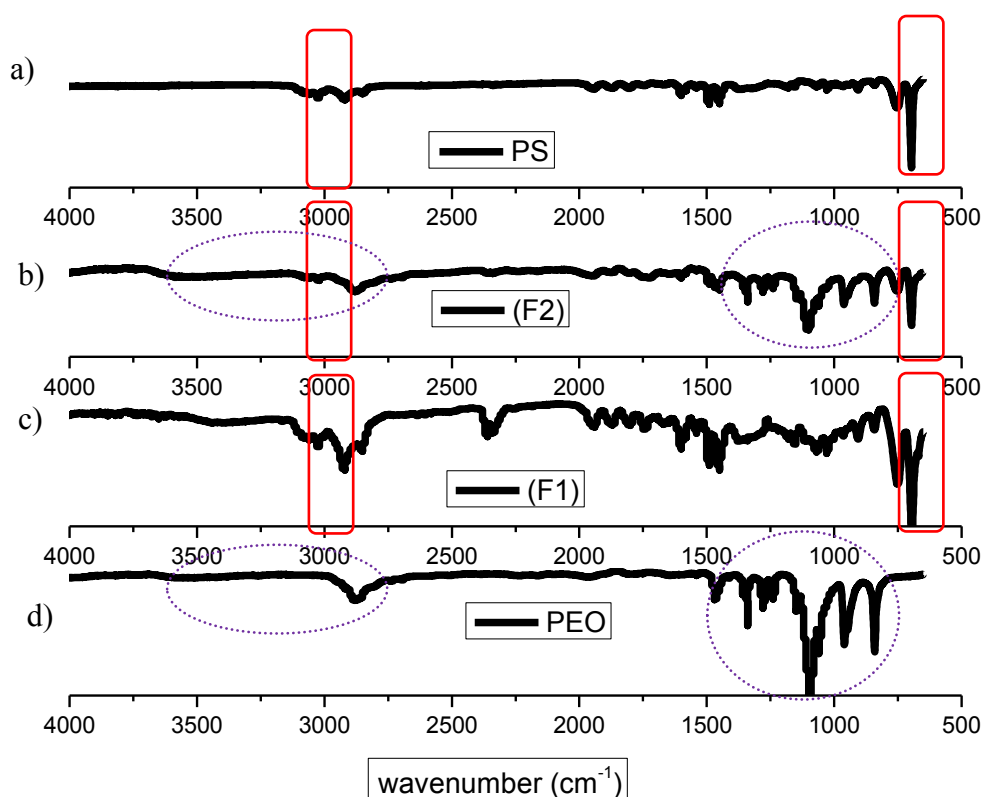


Fig. 4.8 FTIR spectra for (a) PS 132kDa, fractions (b) F1 and (c) F2 of PS-b-PEO 218kDa, and (d) PEO 81.9kDa.

The fractograms of PS-b-PEO 2280kDa copolymer in Figs. 4.9a also show a bimodal distribution. Therefore, this sample was also fractionated again and the fractions subjected to FTIR spectroscopy. Three fractions denoted F1, F2 and F3 (Fig 4.9) were collected for PS-b-PEO 2280kDa copolymer to investigate their chemical structures using FTIR spectroscopy. After the solvent had evaporated from F1 and F2 nothing was left for analysis by FTIR. F2 might have been an impurity that was detected by the MALLS detector as a result of its size.

The FTIR spectrum of the polymeric structure from F3 (Fig 4.10a) shows co-existing peaks for both PS and PEO. At wavenumbers of approximately 700 cm^{-1} (aromatic C-H bend) and 3025 cm^{-1} (aromatic C-H stretch) peaks are present (red rectangles) confirming the presence of PS. In addition to this, the presence of the PEO block was confirmed by peaks at wavenumber $2880\text{--}3000\text{ cm}^{-1}$ (C-H stretch), $3300\text{--}3600\text{ cm}^{-1}$ (O-H stretch) as well as the range of $840\text{--}1360\text{ cm}^{-1}$ (C-O-C stretch). The FTIR spectrum for F3 (Fig 4.10a) confirmed the presence of PS and PEO peaks and can be assigned to the PS-b-PEO 2280 kDa copolymer.

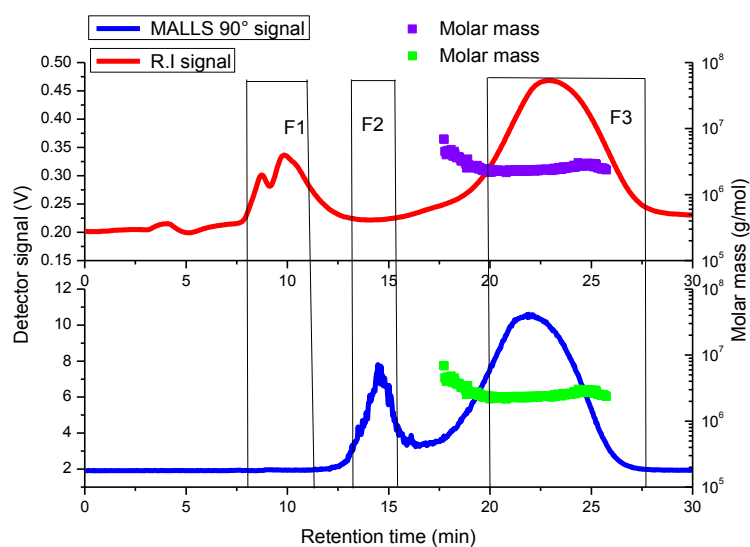


Fig. 4.9 Thermal FFF fractogram of PS-b-PEO 2280 kDa in chloroform showing the RI (red) and MALLS detector signal at 90° (blue) as a function of retention time.

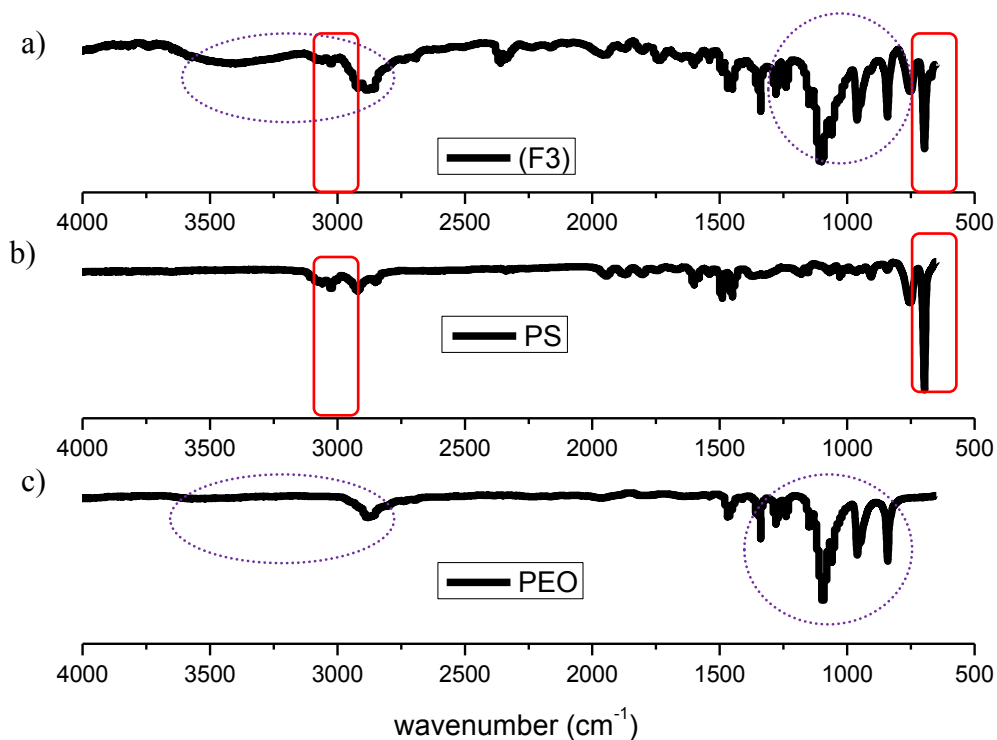


Fig. 4.10 FTIR spectra of (a) Thermal FFF fraction obtained by semi-preparative fractionation of PS-*b*-PEO 2280kDa (F3) copolymer, (b) PS homopolymer (c) PEO homopolymer in chloroform.

4.3 Thermal FFF fractionations in THF

4.3.1 Experimental conditions

In a second set of experiments, PS and PEO homopolymers and the corresponding block copolymers were fractionated in THF as the mobile phase. Different from chloroform, which is a good solvent for both PS and PEO, THF is a selective solvent. THF is a good solvent for PS but a poor solvent for PEO. Accordingly, it is expected that PS will adopt a random coil conformation while PEO will rather form collapsed coils.

All the polymer samples were analyzed at a concentration of 4 mg/ml and a volume of 100 μ l was injected into the channel. The samples were introduced into the channel by manual

injection at a flow rate of 0.2 ml/min for 60 seconds. The focus time was a minute. A constant temperature difference of 70 °C was maintained between hot wall and cold wall for 100 minutes. The cold wall temperature varied between 23 °C and 26 °C. The flow rate was maintained at 0.2 ml/min throughout the runs. The specific refractive index (dn/dc) values used for calculations were 0.072 and 0.185 ml/g for the homopolymers PEO and PS in THF, respectively. The dn/dc of PEO was obtained as mentioned in section 4.2.1. The dn/dc values of the block copolymers were calculated using equation 20

$$\frac{dn}{dc} = w_{PEO} \left(\frac{dn}{dc}_{PEO \text{ in THF}} \right) + w_{PS} \left(\frac{dn}{dc}_{PS \text{ in THF}} \right) \quad (20)$$

where w is the weight fraction of PEO or PS in the block copolymers¹⁰. The corresponding dn/dc values of the block copolymers are shown in Table 4.5.

Table 4.5 dn/dc values for PS-b-PEO copolymers, PEO and PS homopolymers calculated for THF.

Sample name	dn/dc
PS 29.5kDa	0.185
PS 132kDa	0.185
PS 275kDa	0.185
PS-b-PEO 218 kDa	0.129
PS-b-PEO 91.5kDa	0.109
PEO 289kDa	0.072

4.3.2 Analysis of PS and PEO homopolymers by Thermal FFF

The PS samples dissolved readily at room temperature, however, the PEO homopolymers and PS-b-PEO copolymers were insoluble. In order to dissolve them, all the samples were dissolved at 50 °C for 5 hours. These were then injected directly into the Thermal FFF channel at 50 °C before cooling to room temperature. As will be seen, Thermal FFF separated the polymers by both molar mass and chemical composition differences¹.

The superimposed fractograms showing the RI and MALLS signals with the molar mass readings of the PS homopolymers are shown in Figs. 4.11a and b, respectively. An increase

in retention time with increasing molar mass can clearly be seen. This is in agreement with the normal mode of separation for Thermal FFF.

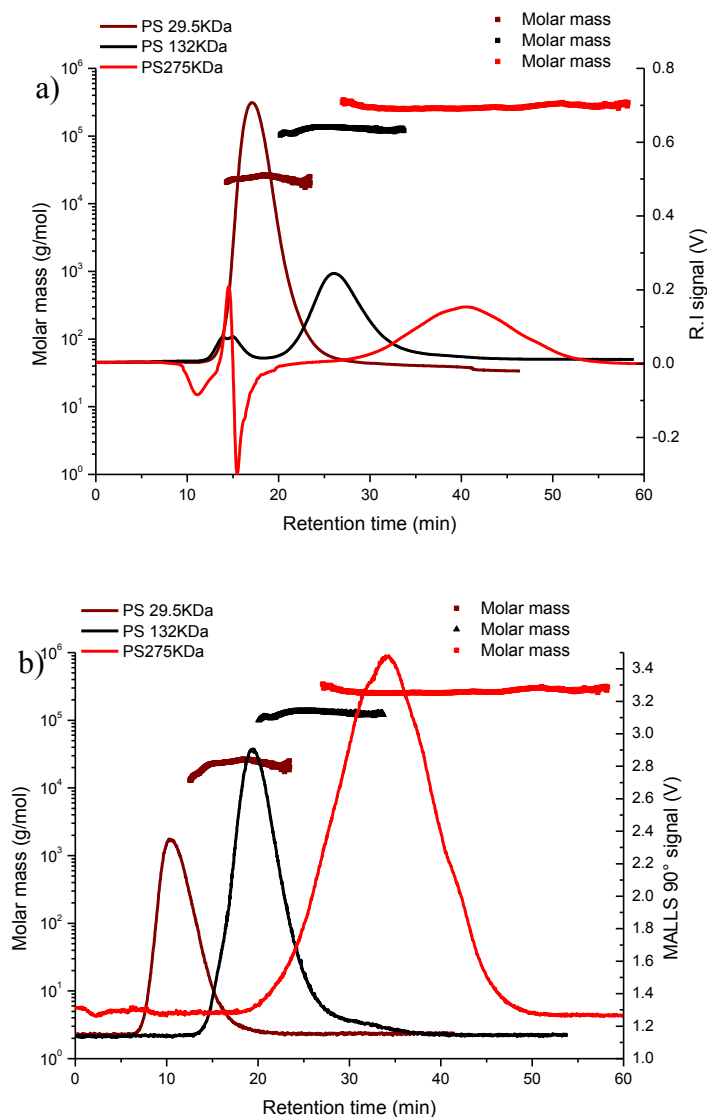


Fig. 4.11 Thermal FFF fractograms of PS homopolymers in THF, (a) RI signal with molar mass overlaid and (b) MALLS 90° signal with molar mass overlaid.

As has been explained before, fractionation in Thermal FFF is a function of the normal (D) and thermal diffusion coefficients (D_T). In the present experiments, the normal diffusion coefficients (D) were determined experimentally. The thermal diffusion coefficient D_T values were then calculated from the obtained D values. Unlike in section 4.2, D_T values could be calculated since the temperature profile throughout the channel was uniform as a result of utilizing the constant temperature programme described in section 4.3.1.

In order to obtain D values, the polymer samples fractionated by Thermal FFF were detected by the DLS detector. The DLS was used to measure the diffusion coefficients of polymers dissolved or dispersed undergoing Brownian motions in a solvent^{30, 54}. From the DLS detector information on the hydrodynamic radius (R_h) of the polymers was obtained. The diffusion coefficients (D) were then calculated from the obtained R_h values using the Stokes-Einstein equation 21

$$D = \frac{kT}{6\pi\eta R_h} \quad (21)$$

Where k is Boltzmann's constant, T is the absolute temperature, and η is the solvent viscosity. The measurements were obtained at a temperature of 25 °C so as to match the Thermal FFF cold wall (T_C) temperature. This was done so as to acquire diffusion measurements at a temperature and polymer concentration that match the Thermal FFF operating conditions.

Substituting equation 7 into equation 13 and using the D values obtained from equation 21, the thermal diffusion coefficients (D_T) were calculated using equation 22

$$D_T = \frac{6Dt_r}{t_0\Delta T} \quad (22)$$

where ΔT is the temperature difference applied across the channel thickness assuming a constant gradient, D is the diffusion coefficient, t_0 retention time of an unretained component and t_r retention time of the solute.

The diffusion coefficients (D) together with the calculated molar masses are summarized in Table 4.6.

Table 4.6 Molar masses, D and D_T values for PS and PEO determined by Thermal FFF in THF.

Sample name	D*10 ⁻⁷ (cm ² /s)	D _T *10 ⁻⁷ (cm ² /s K)	M _w (g/mol)	M _n (g/mol)
PS 29.5kDa	7.93	0.633	20 570	22 350
PS 132kDa	3.30	0.463	127 000	107 000
PS 275kDa	2.00	0.476	264 900	263 900
PEO 289kDa	1.97	0.335	70 040	60 860

As can be expected, D decreases with increasing molar mass. In contrast, D_T is higher for the lower molar mass PS homopolymer sample but is more or less identical for higher molar mass samples. This indicates that D_T becomes independent from molar mass if the molar mass is sufficiently high. In these cases the separation is mainly a function of D. The obtained D_T values shown in Table 4.6 are lower than those from literature¹¹, this might have been due to errors in the determination of D values. It is interesting to note that D is similar for PS and PEO of similar molar mass while D_T is different.

Similar to the fractionations in chloroform, the molar masses for PS homopolymers determined in THF agree quite well with the nominal molar masses. This is another proof for the fact that THF is a thermodynamically good solvent for PS.

The PEO homopolymers were analysed using the same experimental conditions. For the lower molar mass samples (44.3kDa and 81.9kDa) very noisy MALLS signals were obtained. This was partially due to poor solubility of PEO in THF. In order to obtain good MALLS signals, the concentration of the samples was gradually increased from 4 mg/ml to 10 mg/ml. No significant change in the MALLS signals was observed. When the concentration was 10 mg/ml the channel blocked due to overloading. The fractograms of PEO 289kDa together with a PS homopolymer of a similar molar mass are presented in Fig. 4.12.

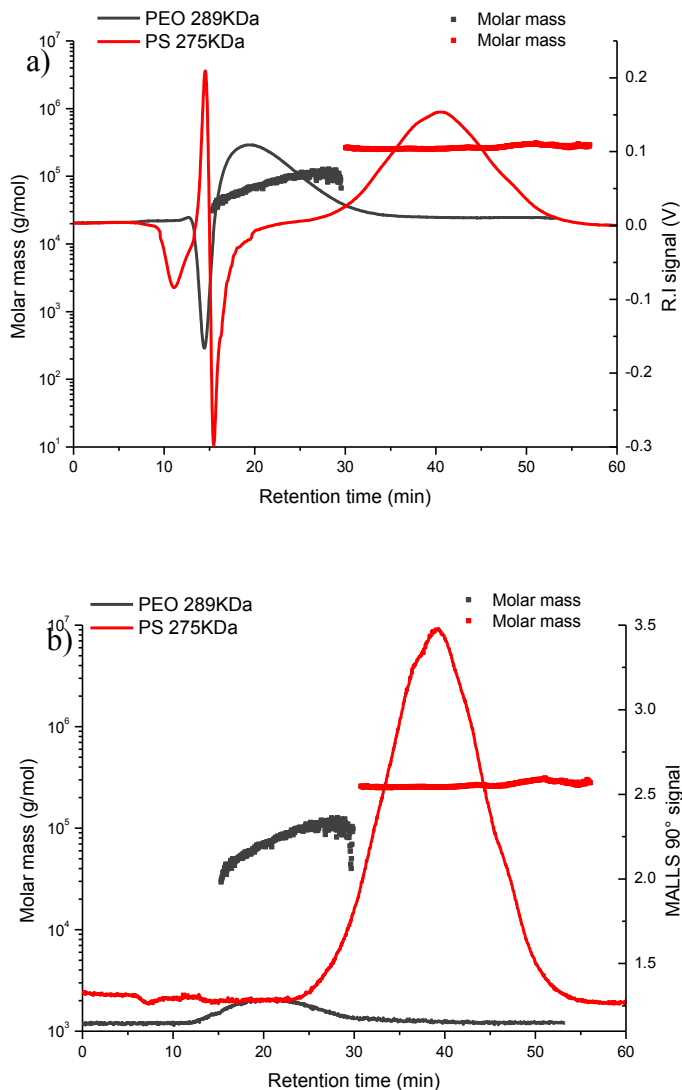


Fig. 4.12 Thermal FFF fractograms of PS and PEO in THF, (a) RI signal with molar mass overlaid and (b) MALLS 90° signal with molar mass overlaid. Samples PS 275 kDa and PEO 289 kDa.

Although both samples have similar molar masses, their Thermal FFF behaviour is distinctively different. PEO elutes before PS and the molar mass reading indicates a significantly lower molar mass. As is shown in Table 4.6, D_T of PEO is significantly lower as compared to PS. This explains the early elution of this sample. Another important factor is that THF is a rather poor solvent for PEO as has been discussed before. This means that coil expansion is rather low and the hydrodynamic volume in THF is lower than the hydrodynamic volume in a good solvent (chloroform). THF is a very good solvent for PS and, therefore, the polymer coils are well expanded. Considering the effect of coil expansion as a function of solvent quality the early elution of PEO can be understood.

4.3.3 Fractionation of PS-b-PEO copolymers by Thermal FFF with THF and comparison with PS and PEO homopolymers

As has been seen in the previous section, the elution behaviour of PS and PEO in THF are distinctively different. PS adopts a random coil conformation while PEO is present probably as a collapsed coil. It is now interesting to investigate the behaviour of the PS-b-PEO copolymers where both conformations are combined to each other.

The lower molar mass samples PS-b-PEO copolymers 1 and 2 shown in Table 3.2 co-eluted using the above mentioned temperature programme in THF. This might be due to the presence of PS blocks with molar masses below 10 kDa in the block copolymers. These low molar mass PS blocks in the block copolymers are difficult to separate using single component solvents which have a limited effect on polymer retention in Thermal FFF. Very noisy MALLS peaks were also obtained. Upon gradually increasing the polymer concentration from 4-10 mg/ml, the Thermal FFF channel blocked as a result of sample overloading without a significant noise reduction. For the higher molar mass block copolymers these problems were not encountered. Some were analysed together with PS and PEO homopolymers that had molar masses identical to the block molar masses or the total molar masses.

For PS-b-PEO 91.5 kDa copolymer (PEO block 61.5 kDa, PS block 30 kDa), PS 29.5 kDa was selected to represent the PS block and PS 132 kDa to represent the total molar mass of the block copolymer.

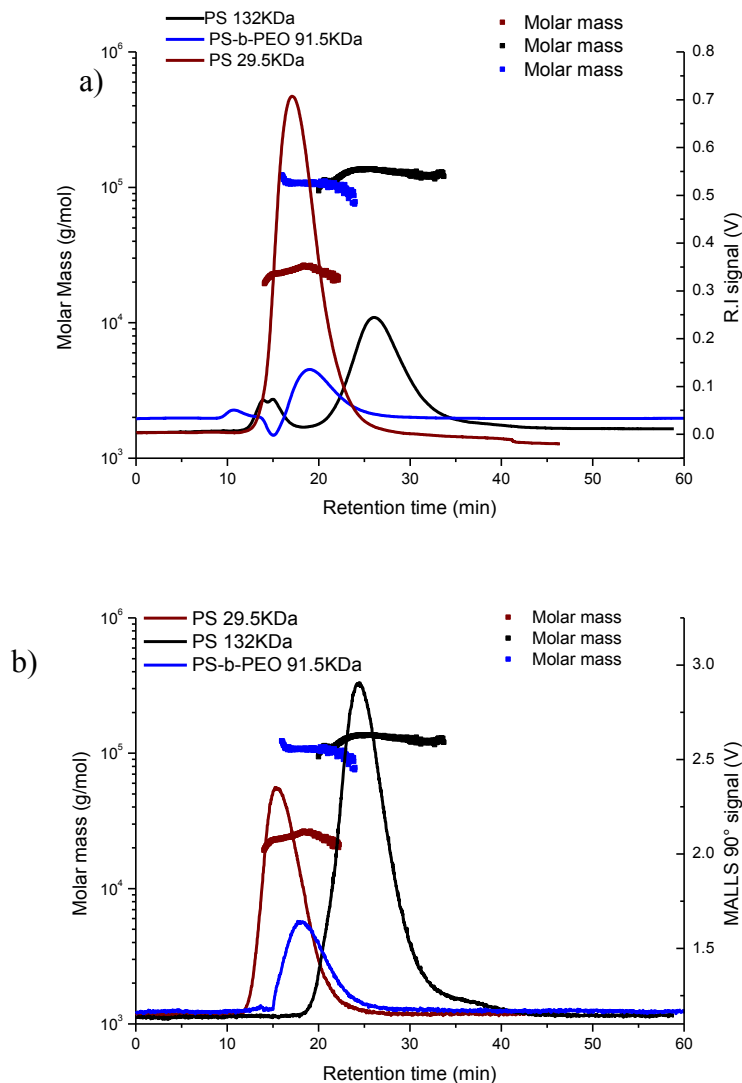


Fig. 4.13 Thermal FFF fractograms of PS and PS-b-PEO in THF. (a) RI signal with molar mass overlaid, (b) MALLS 90° signal with molar mass overlaid. Samples PS-b-PEO 91.5 kDa, PS 29.5 kDa and PS 132 kDa.

Figs. 4.13a and b provide some very interesting observations. The two PS samples elute according to expectations with the lower molar mass sample eluting first followed by the higher molar mass sample. The block copolymer sample elutes at roughly the same elution time as the low molar mass PS sample. The molar mass of the PS (29.5 kDa) is roughly the same as the molar mass of the PS block (30 kDa) of the block copolymer. This indicates that the retention of PS-b-PEO copolymer in THF is dependent on the molar mass of the PS block. This happens because in THF, PS is in a good solvent and can expand freely¹⁴. As for the PEO block it can be assumed that it adopts a rather collapsed coil conformation and does

not significantly contribute to the diffusion coefficient (D). This is in agreement with the results shown in Table 4.6 and 4.7 summarizing the diffusion coefficients and the calculated molar masses for the homopolymers and block copolymers, respectively.

Table 4.7 Molar masses, D and D_T values for the block copolymers analysed in THF.

Sample name	$D \cdot 10^{-7}$ (cm^2/s)	$D_T \cdot 10^{-7}$ ($\text{cm}^2/\text{s K}$)	M_w (g/mol)	M_n (g/mol)
PS-b-PEO 218 kDa	3.33	0.414	177 000	169 000
PS-b-PEO 91.5 kDa	5.47	0.609	105 400	97 530

Comparing Tables 4.6 and 4.7 it can be seen that the thermal diffusion coefficients (D_T) of PS and the block copolymer are practically identical (0.633 and $0.609 \times 10^{-7} \text{ cm}^2/\text{sK}$, respectively). This proves that PS and the block copolymer have the same surface chemical composition in solution. The elution behaviours of PS-b-PEO 218 kDa copolymer (PEO block 109 kDa, PS block 109 kDa) and the corresponding PS and PEO homopolymers with related molar masses are compared in Figs. 4.14a and b. Here, a similar picture is obtained showing that PS is co-eluting with the PS-b-PEO 218 kDa copolymer. This indicates again that retention of the block copolymer is determined mainly by the molar mass of the PS block. The D values of PS 132 kDa and the block copolymer reflect the stronger influence of the molar mass (3.30 and $3.33 \times 10^{-7} \text{ cm}^2/\text{s}$ respectively).

a)

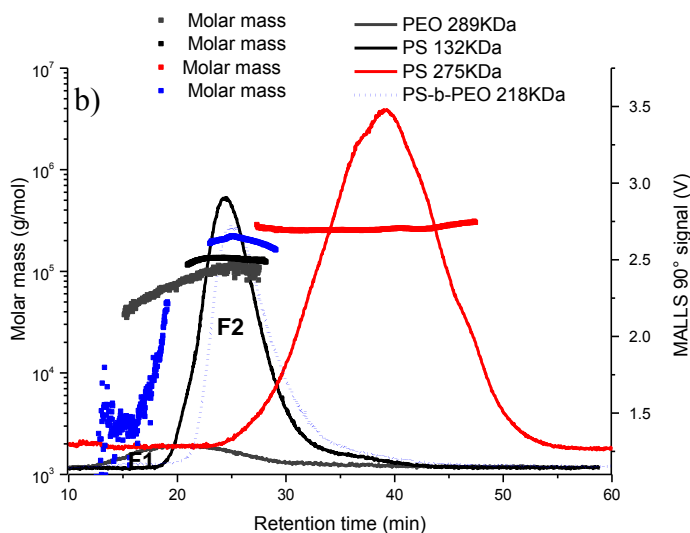
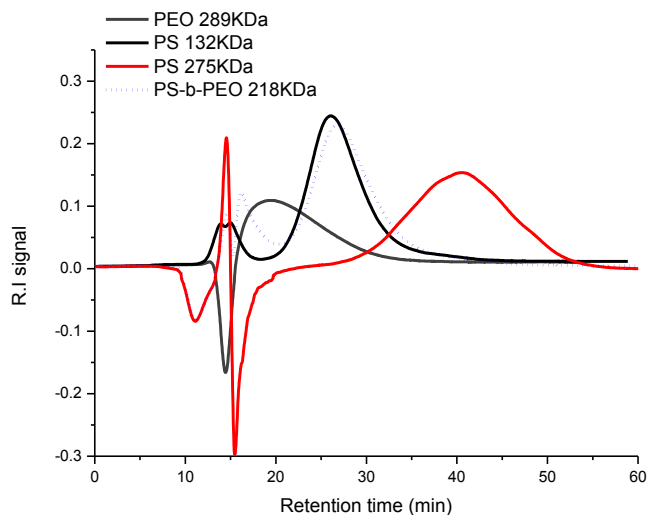


Fig. 4.14 Thermal FFF fractograms in THF, (a) RI signal with molar mass overlaid, (b) MALLS 90° signal with molar mass overlaid. Samples: PS 132 kDa and 275 kDa, PEO 289 kDa and PS-b-PEO 91.5 kDa copolymer.

The PS 132 kDa and the bulk PS-b-PEO 218 kDa copolymer D_T values are very close as shown in Tables 4.6 and 4.7 (0.463 and $0.414 \times 10^{-7} \text{ cm}^2/\text{sK}$ respectively). This proves that the D_T values are rather independent of molar mass but dependent on the surface chemical composition in solution^{1, 14, 17}. Hence, PS 132 kDa and PS-b-PEO 218 kDa copolymer have the same surface chemical composition.

It can, therefore, be assumed that the PEO block behaves as mentioned above. Another interesting observation is that PEO 289 kDa elutes earlier than PS 275 kDa as shown in Figs. 4.14a and b indicating again that retention is dependent on chemical composition and coil conformation but not primarily molar mass.

The PS-*b*-PEO 218 kDa copolymer was separated into two main fractions (denoted F1 and F2) as shown in Figs.4.15a and b. From the fractograms, it can be seen that F1 (first fraction obtained) had a significantly lower molar mass than F2 (second fraction obtained). FTIR spectroscopy was utilized to determine the chemical composition of F1 and F2.

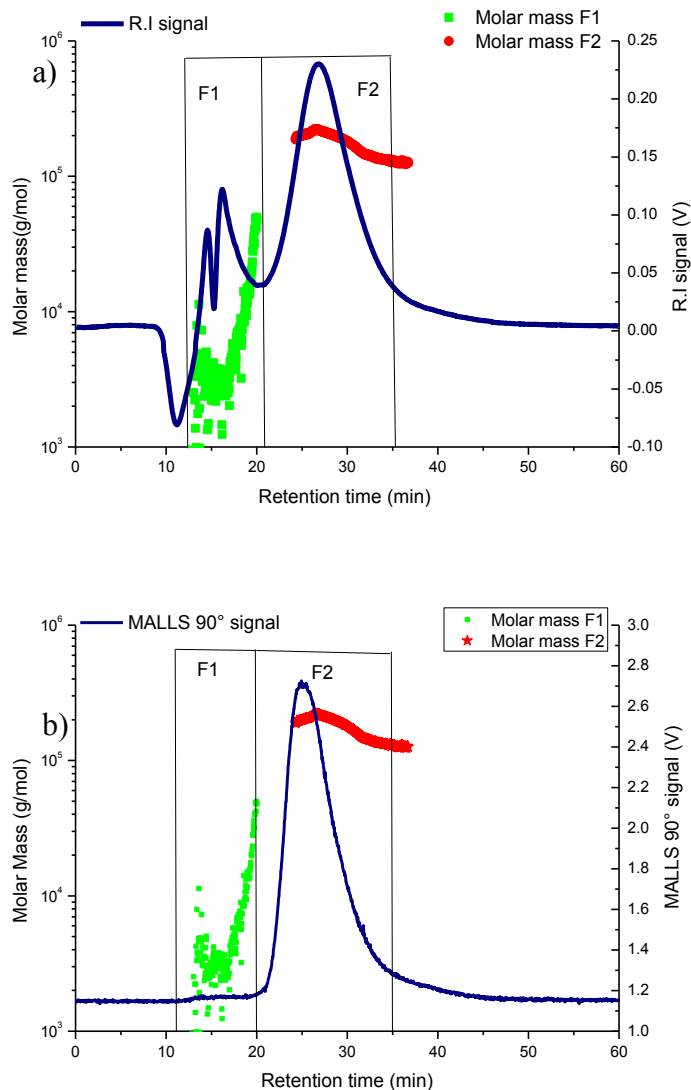


Fig. 4.15 Thermal FFF fractogram of PS-b-PEO 218kDa copolymer in THF. (a) RI signal with molar mass overlaid, (b) MALLS 90° signal with molar mass overlaid.

From the fractogram in Fig. 4.16, F1 can be assigned to the PEO homopolymer due to the absence of a UV signal at 254 nm, signifying the absence of PS which is UV active at this wavelength. The major eluting component in F2 shows RI, UV and MALLS detector signals at the same retention time and can be assigned to the PS-b-PEO copolymer. The MALLS signal is much more intense compared to F1, which indicates the presence of polymer with a higher molar mass.

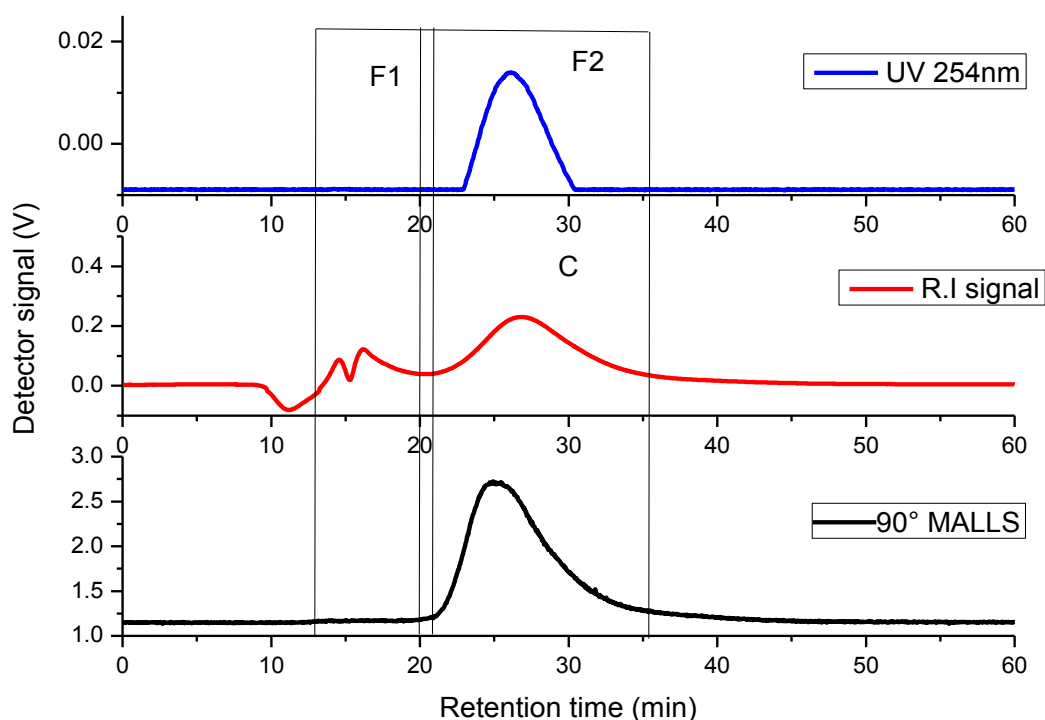


Fig. 4.16 Thermal FFF fractogram of PS-b-PEO 218 kDa copolymer showing the UV 254 nm (blue), RI signal (red) and MALLS detector signal at 90° (black) as a function of retention time in THF.

4.3.4 Qualitative FTIR analysis of the separated components of PS-b-PEO 218 kDa block copolymer

The FTIR spectra of the separated components of PS-b-PEO 218 kDa copolymer are shown in Figs. 4.17a and b. The FTIR spectrum of the first polymeric structure F1 shows main peaks similar to those found for PEO 81.9 kDa at wavenumbers of 2880-3000 cm^{-1} (C-H stretch), 3300-3600 cm^{-1} (O-H stretch) as well as the range of 840–1360 cm^{-1} (C-O-C stretch). These peaks are highlighted by purple circles in Fig 4.17d. Therefore, F1 (Fig 4.17b) can be assigned to a PEO homopolymer. The FTIR spectrum of the second polymeric structure F2 (Fig4.17a) shows co-existing peaks for both PS and PEO. At wavenumbers of approximately 700 cm^{-1} (aromatic C-H bend) and 3025 cm^{-1} (aromatic C-H stretch) peaks for PS (red rectangles) appear in addition to those mentioned above for PEO homopolymer (purple circles). Therefore, F2 shown in Fig. 4.17a can be assigned PS-b-PEO copolymer.

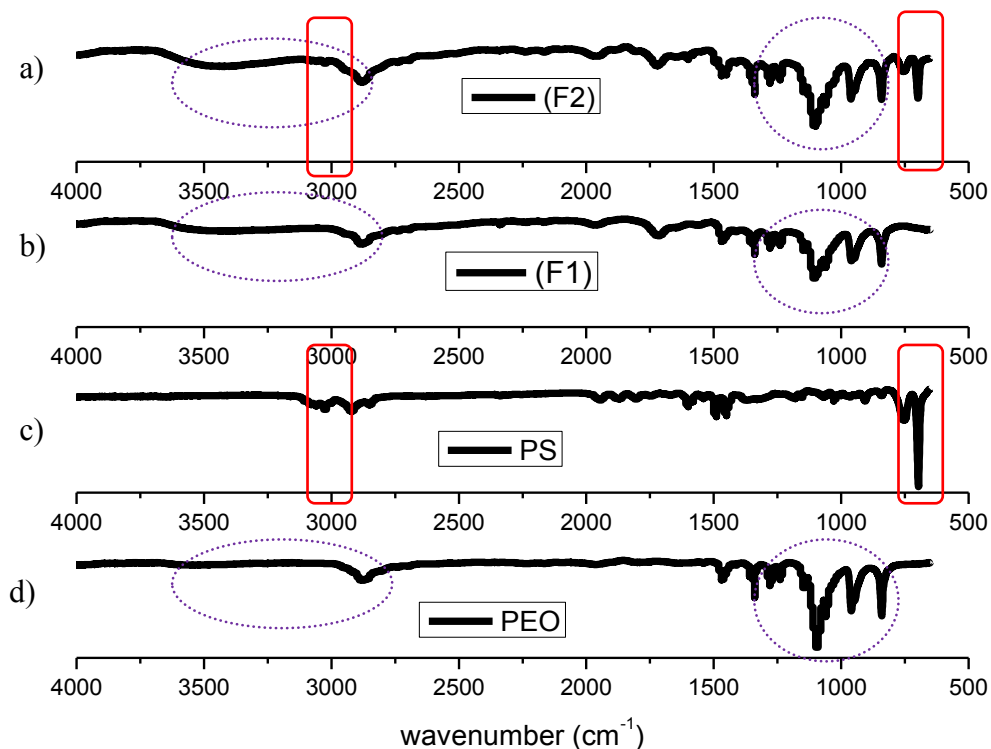


Fig. 4.17 FTIR spectra for fractions F1 and F2 (bulk sample) of PS-b-PEO 218 kDa copolymer, PEO 81.9 kDa and PS 132 kDa.

4.4 Thermal FFF fractionations in toluene

In this section toluene as a selective solvent for PS is used to investigate the FFF behaviour of PS-b-PEO copolymers. The elution behaviour and separation of the PS and PEO homopolymers was also investigated. The PS homopolymer samples dissolved readily at room temperature, however the PEO homopolymers and PS-b-PEO copolymers were insoluble. The constant temperature programme with a ΔT of 70 °C described in section 4.3.1 was applied to these polymer samples. They were dissolved as mentioned in section 4.3.2. The dn/dc of PEO was estimated from its dn/dc value in methanol and differences of the refractive indices of methanol and toluene¹⁰. The dn/dc values of the block copolymers were calculated using the following equation 23:

$$\frac{dn}{dc} = w_{PEO} \left(\frac{dn}{dc}_{PEO \text{ in Toluene}} \right) + w_{PS} \left(\frac{dn}{dc}_{PS \text{ in Toluene}} \right) \quad (23)$$

where w is the weight fraction of PEO or PS in the block copolymers¹⁰. The corresponding dn/dc values of the block copolymers are shown in Table 4.8.

Table 4.8 dn/dc values for PS-*b*-PEO copolymers, PEO and PS homopolymers calculated for toluene.

Sample name	dn/dc
PS 29.5 kDa	0.098
PS 132 kDa	0.098
PS- <i>b</i> -PEO 91.5 kDa	0.019
PS- <i>b</i> -PEO 218 kDa	0.042
PEO 81.9 kDa	-0.02

4.4.1 Fractionation of PS homopolymers by Thermal FFF in toluene.

The fractograms showing the RI and MALLS signals with the molar mass of the PS homopolymers are shown in Figs. 4.18a and b, respectively. An increase in retention time

with increase in molar mass can clearly be seen. This shows the normal mode of separation in Thermal FFF. PS homopolymers were separated according to their molar mass. The polymer D and D_T values were calculated using equations 21 and 22 respectively. Online measured D values shown in Table 4.9 were used to calculate the D_T values of the PS homopolymers. The D values of PS 29.5 kDa and PS 132 kDa are significantly different (6.37 and $3.61 \times 10^{-7} \text{ cm}^2/\text{s}$, respectively). As expected, the D values decrease with increase in molar mass, thus showing a dependence on molar mass. These two homopolymers have the same chemical composition and, accordingly, their D_T values shown in Table 4.9 are practically identical (0.118 and $0.120 \times 10^{-7} \text{ cm}^2/\text{sK}$ respectively).

The D_T values of PS homopolymers vary insignificantly with increase in molar mass. The D_T values for the PS homopolymers in toluene and THF are different, (see Table 4.9 and 4.6, respectively). This proves that D_T depends on the chemical composition of the polymer-solvent system¹¹ and not on that of the polymer only.

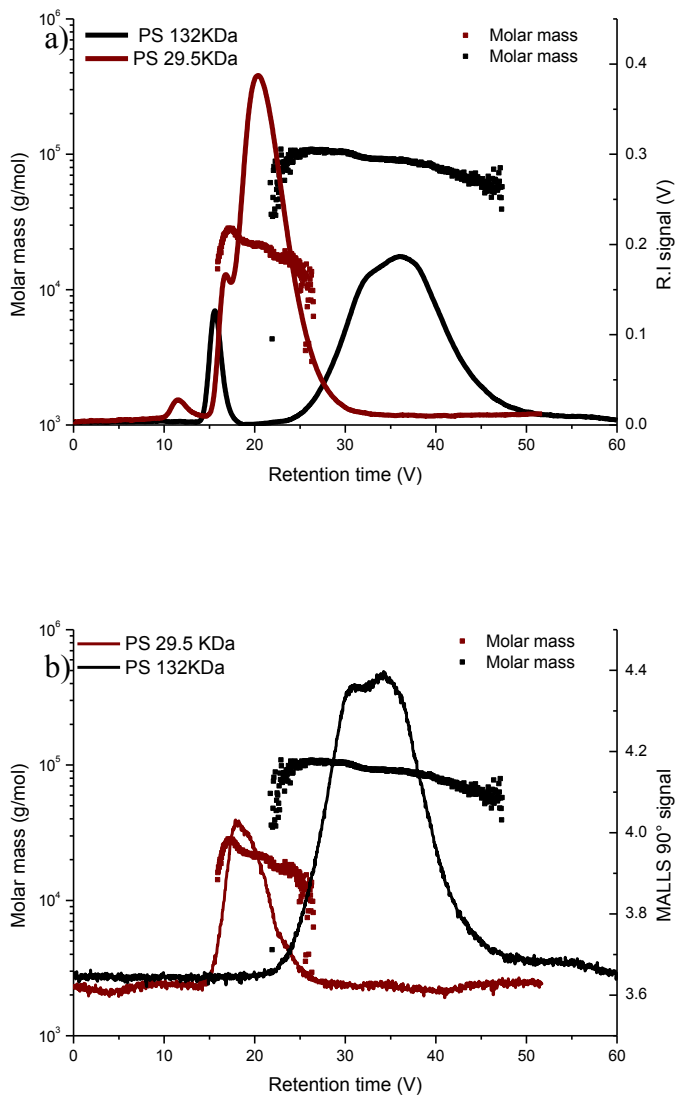


Fig. 4.18 Thermal FFF fractograms of PS homopolymers in toluene using a constant temperature gradient, (a) RI signal with molar mass overlaid and (b) MALLS 90° signal with molar mass overlaid. Samples PS 29.5 kDa and PS 132 kDa.

Table 4.9 Molar masses, D and D_T for polymers analysed in toluene

Sample name	$D \cdot 10^{-7}$ (cm^2/s)	$D_T \cdot 10^{-7}$ ($\text{cm}^2/\text{s K}$)	M_w (g/mol)	M_n (g/mol)
PS 29.5 kDa	6.37	0.118	20 650	21 460
PS 132 kDa	3.61	0.12	90 910	88 900
PS-b-PEO 91.5 kDa	6.16	0.128	110 300	74 630
PS-b-PEO 218 kDa	3.36	0.104	222 000	218 800

4.4.2 Fractionation of PS-b-PEO copolymers by Thermal FFF and comparison with PS and PEO homopolymers.

PEO homopolymers could not be fractionated under the present conditions. The PEO homopolymers were injected into the channel, however, no peak was observed at a concentration of 4 mg/ml in both the MALLS and RI during the entire period of the experimental run. The PEO homopolymer concentration was gradually increased to try to improve the detection. Upon increasing the concentration of PEO 44.3 kDa to 8 mg/ml the channel blocked due to overloading.

The fractograms of PS and PS-b-PEO's FFF behaviour are shown in Figs. 4.19a and b. Again molar mass combinations were selected that reflect the total molar masses of the block copolymer and the PS block. The two PS samples elute in the expected order with the lower molar mass sample (PS 29.5 kDa) eluting first, followed by the higher molar mass sample (PS 132 kDa). In contrast to the behaviour in chloroform and THF, the molar masses that were obtained by Thermal FFF deviated significantly from the nominal molar masses.

The fractionation behaviour of the block copolymers followed a trend that has been seen before. The PS 29.5 kDa homopolymer and PS-b-PEO 91.5 kDa copolymer elute roughly at the same time, as seen by the RI and MALLS 90° signals. This indicates that retention of PS-

b-PEO 91.5 kDa copolymer in toluene is dependent on the molar mass of the PS block in the block copolymer.

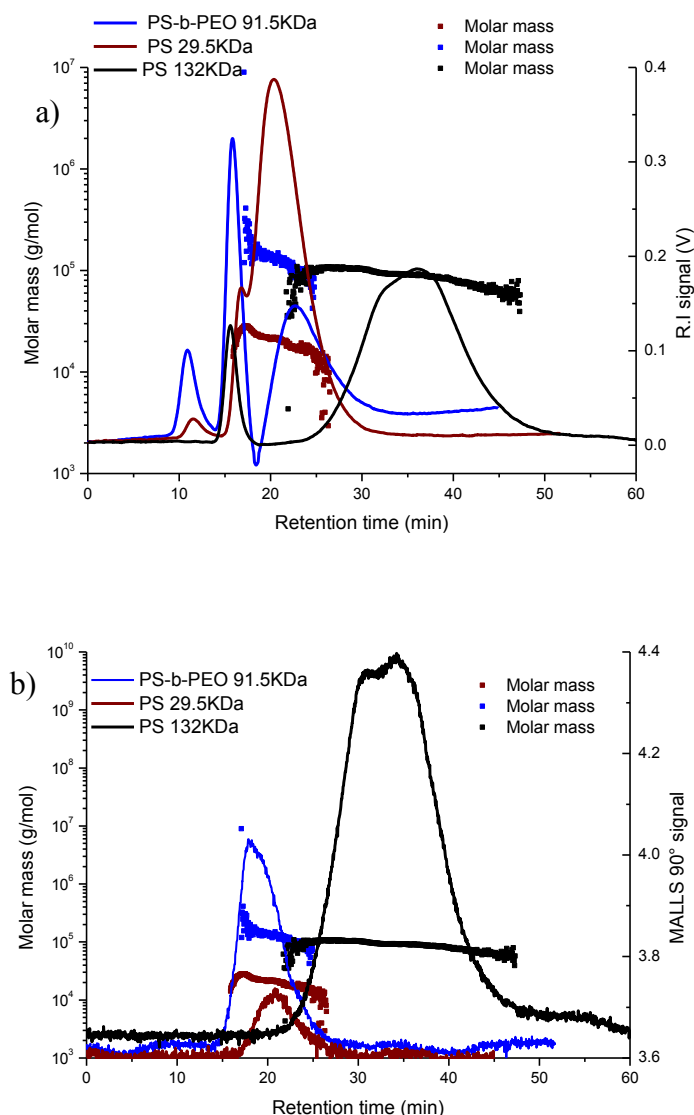


Fig. 4.19 Thermal FFF fractograms in toluene using a constant temperature gradient. (a) RI signal with molar mass overlaid and (b) MALLS 90° signal with molar mass overlaid. Samples PS 29.5 kDa, PS 132 kDa and PS-b-PEO 91.5 kDa copolymer.

Similar to THF it can be assumed that in toluene (as a selective solvent for PS) the PS block adopts an expanded coil conformation¹⁴. The PEO block is assumed to adopt a rather collapsed coil conformation and does not significantly contribute to the diffusion coefficient and the size of the macromolecules in solution. This is evidenced by the D values of PS homopolymer and PS-b-PEO copolymer which vary insignificantly as shown in Table 4.9 (6.37 and $6.16 \times 10^{-7} \text{ cm}^2/\text{s}$ for PS 29.5 kDa and PS-b-PEO 218 kDa, respectively). Their

calculated D_T values vary insignificantly, thus proving that PS-b-PEO 91.5 kDa and PS 29.5 kDa copolymer have the same surface chemical composition in toluene (0.128 and $0.118 \times 10^{-7} \text{ cm}^2/\text{s K}$ respectively). Accordingly, D_T is governed by the PS block in the block copolymer in toluene since it is a good solvent for PS^{1, 14}.

The elution behaviour of PS-b-PEO 218 kDa copolymer (PEO 109 kDa, PS 109 kDa) and PS 132kDa homopolymer are compared in Figs 4.20a and b. The RI and MALLS 90° signals of PS-b-PEO 218 kDa copolymer and PS 132 kDa closely overlap. The D values of PS-b-PEO 218 kDa copolymer and PS 132 kDa are practically identical (3.61 and $3.36 \times 10^{-7} \text{ cm}^2/\text{s}$ for PS and PS-PEO, respectively); this proves that PEO does not significantly contribute to the block copolymer's diffusion coefficient. PS 275 kDa eluted later than PS-b-PEO 218 kDa copolymer, however very broad bimodal peaks were obtained for PS 275 kDa. The RI peak (PS 275 kDa) was almost lost in the baseline. Upon trying to use temperature programmes with low constant temperature differences between the hot wall and the cold wall (ΔT), no significant change was noted from the fractograms. Such low temperature differences reduce the retention time of the polymer in the channel, thus minimizing peak broadening. As a result of this, there was need for a new method to be developed.

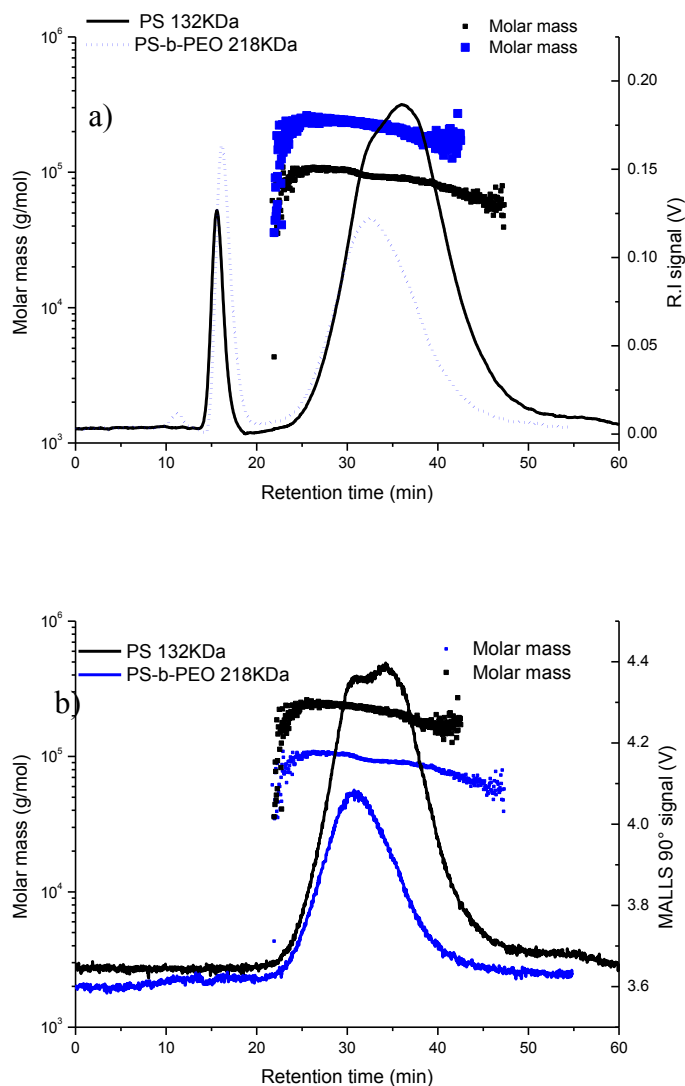


Fig. 4.20 Thermal FFF fractograms in toluene using a constant temperature gradient. (a) RI signal with molar mass overlaid and (b) MALLS 90° signal with molar mass overlaid. Samples PS 132 kDa and PS-b-PEO 218 kDa copolymer.

4.4.3 Fractionation of PS-b-PEO copolymers and PS and PEO homopolymers by Thermal FFF in toluene using a linear temperature programme.

In order to best characterize polymers with high molar masses, the reverse programmed temperature gradient mentioned in section 4.2 was also used. This was utilized so that polymers with high molar masses would elute within reasonable times²¹. An initial temperature difference between the hot wall and the cold wall of 40 °C was used, which

decreased with time to a final temperature difference of 0 °C as shown in Fig. 4.1. The cold wall temperature (T_C) varied between 23-26 °C.

Table 4.10 Molar masses and dn/dc values for PS homopolymers and PS-b-PEO copolymers analysed in toluene using a programmed temperature gradient.

Sample name	M_w (g/mol)	M_n (g/mol)	dn/dc
PS 132 kDa	140 600	139 700	0.098
PS 275 kDa	279 700	275 100	0.098
PS 1412 kDa	1 256 000	1 252 000	0.098
PS-b-PEO 218 kDa	204 300	206 300	0.042
PS-b-PEO 2280 kDa	3 411 000	3 374 000	0.039

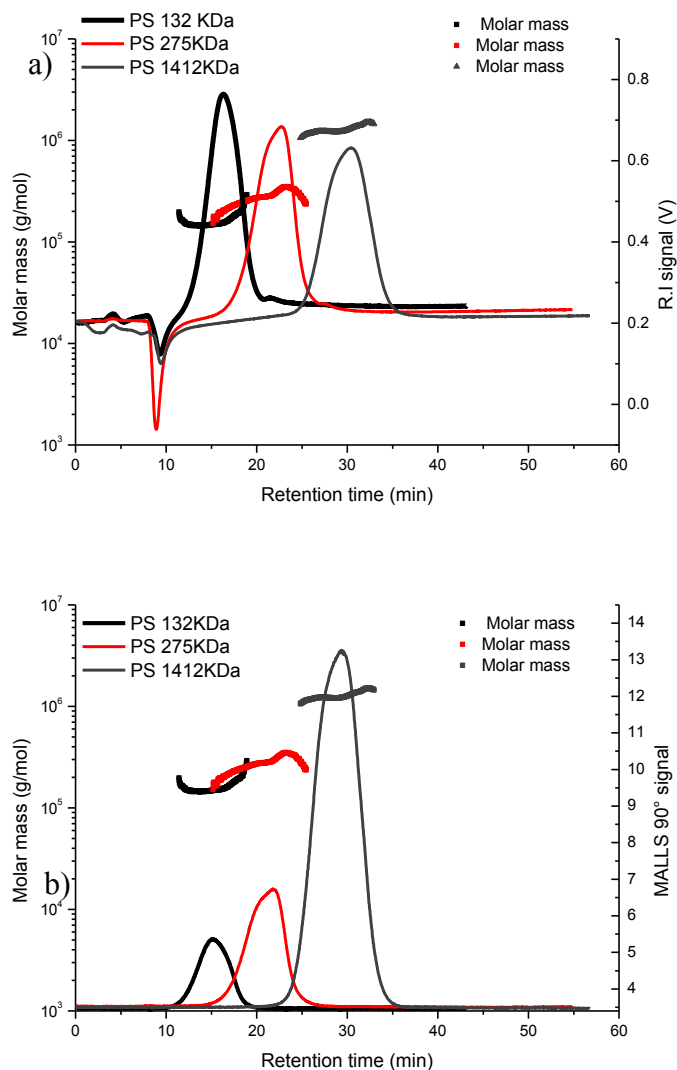


Fig. 4.21 Thermal FFF fractograms in toluene using a programmed temperature gradient. (a) RI signal with molar mass overlaid and (b) MALLS 90° signal with molar mass overlaid. Samples PS 132 kDa, PS 275 kDa and PS 1412 kDa.

The PS homopolymer fractograms in Figs 4.21a and b show an increase in retention time with increase in molar mass. This shows the normal mode of separation in Thermal FFF. An interesting observation is that at a high-temperature gradient (see in Fig. 4.1) the low molar mass PS homopolymer elutes. As the gradient drops to lower temperatures the high-molar mass PS homopolymer then elutes²². It can be seen that the reverse programmed temperature gradient was suitable for the separation of polymers that span over a broad molar mass range in a single experiment.

4.4.4 Fractionation of PS-b-PEO copolymers and comparison to PS and PEO homopolymers.

As can be seen in Figs. 4.22a and b, the fractograms of PS 132 kDa and PS-b-PEO 218 kDa copolymer closely overlap. This proves that retention of PS-b-PEO 218 kDa copolymer in toluene is mostly influenced by the molar mass of the PS block in the block copolymer. As mentioned above toluene is a good solvent for PS, the PS block expands freely and it is assumed to form a random coil conformation. However the PEO block is assumed to behave similarly in both THF and toluene. Another interesting observation is that although a constant temperature and a reversed gradient temperature programme have been utilized to analyse polymers in toluene, similar FFF behaviours of the polymers are observed. However, when a reverse gradient temperature programme is used, the analysis time is short due to a rapid decrease in temperature with time.

Despite the inability to quantitatively determine D_T values of the polymers using a programmed temperature gradient, narrow peaks of PS 275 kDa were successfully obtained in the same experiment. PS 132 kDa and PS 275 kDa elute in the expected order from low to high molar mass with increasing retention time. This indicates the Thermal FFF normal mode of separation.

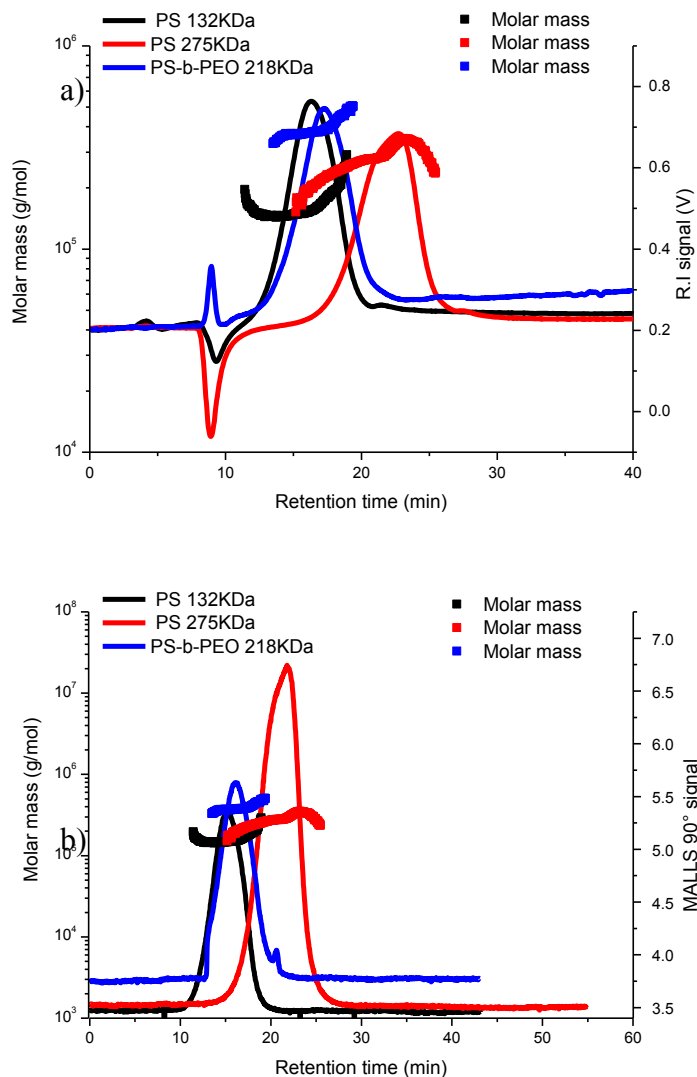


Fig. 4.22 Thermal FFF fractograms in toluene using a programmed temperature gradient. (a) RI signal with molar mass overlaid and (b) MALLS 90° signal with molar mass overlaid. Samples PS 132 kDa, PS 275 kDa and PS-b-PEO 218 kDa copolymer.

The fractograms in Figs. 4.23a and b show a trend similar to the one in Figs. 4.22a and b above. From the fractograms, we can observe that the elution behaviour of PS-b-PEO copolymers in a good solvent for PS is determined by the molar mass of the PS in the block copolymer despite the temperature program used.

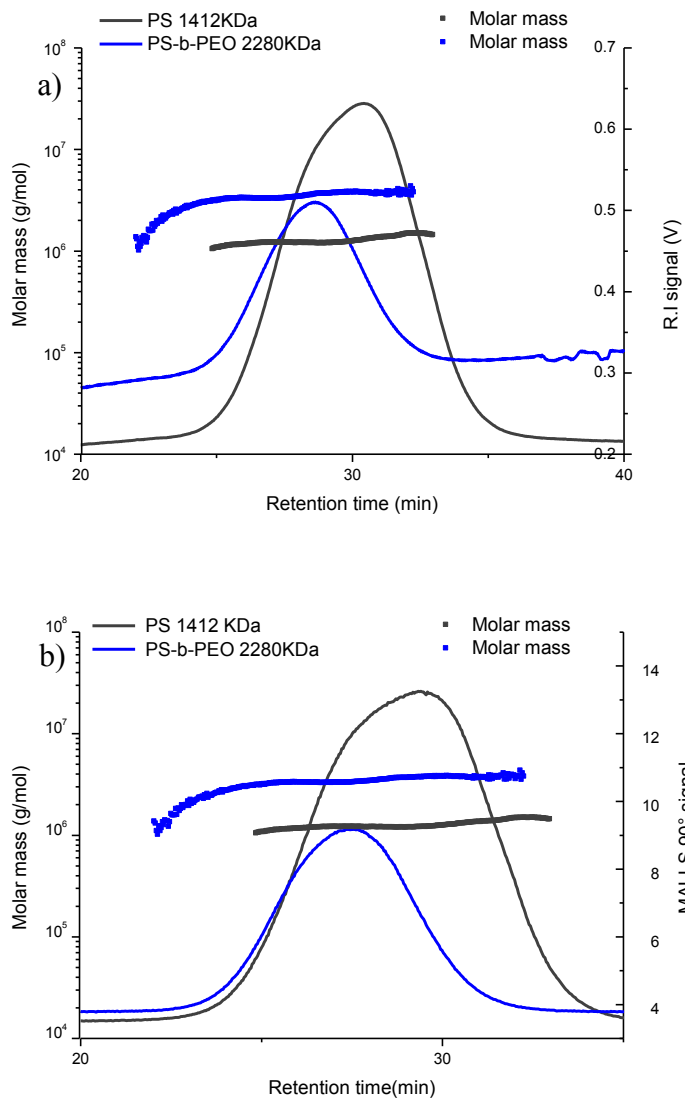


Fig. 4.23 Thermal FFF fractograms in toluene using a programmed temperature gradient . (a) RI signal with molar mass overlaid and (b) MALLS 90° signal with molar mass overlaid. Samples PS 1412 kDa and PS-b-PEO 2280 kDa copolymer.

4.5 Analysis of PS-b-PEO copolymers, PS and PEO homopolymers by AF4 coupled to MALLS-RI detection

4.5.1 Analysis conditions

PS-b-PEO copolymers are amphiphilic polymers. The PS and PEO blocks have different affinities for different solvents²⁴. The elution behaviour and molar mass distribution of PS-b-PEO copolymers as well as PS and PEO homopolymers with related molar masses was investigated using AF4 as an alternative to Thermal FFF. AF4 separates macromolecules according to differences in hydrodynamic size²⁵. In our study chloroform as a good solvent for both PEO and PS homopolymers was used. The results were compared to those obtained in section 4.2, where chloroform was used in Thermal FFF.

The samples were introduced into the channel by manual injection with a tip flow rate of 0.2 ml/min for a time of 4 min. While the samples were being injected, the cross flow was kept constant at 2.0 ml/min and the focus flow was automatically adjusted to 2.3 ml/min in order to maintain a constant detector flow of 0.5 ml/min. After injection the focus flow rapidly decreased to zero, while the tip flow increased to 2.5 ml/min. After 2.5 min, the cross-flow and the tip flow decreased gradually to a value of 0.01 and 0.51 ml/min, respectively. The specific refractive index values used for calculations were 0.027 and 0.185 ml/g for homopolymers of PEO and PS in chloroform, respectively. The dn/dc values of the block copolymers were calculated using equation 19. The corresponding dn/dc value of the block copolymers are shown in Table 4.11.

Table 4.11 Molar masses and dn/dc values for PS-b-PEO copolymers, PS and PEO homopolymers in chloroform as determined by AF4.

Sample name	M_w (g/mol)	M_n (g/mol)	dn/dc
PS 132 kDa	173 700	126 100	0.14
PS 275 kDa	273 900	256 300	0.14
PS 1412 kDa	1 100 000	1 012 000	0.14
PEO 289 kDa	14 270 000	1 129 000	0.027
PEO 1015 kDa	12 900 000	5 145 000	0.027
PS-b-PEO 218 kDa	336 800	336 800	0.084
PS-b-PEO 2280 kDa	1 745 000	1 714 000	0.079

4.5.2 Analysis of PS-b-PEO copolymers, PS and PEO homopolymers by AF4 in chloroform.

Upon trying to analyse PEO homopolymers using the above method, they showed strong interaction with the regenerated cellulose membrane. This might have been due to the interaction of the C-O-C and the O-H groups of PEO with the C-O-H groups of the regenerated cellulose membrane. Figs 4.24b show the MALLS 90 °C signal for the PEO 289kDahomopolymer with the molar mass plot. It can be clearly seen that adsorption occurred. The MALLS 90° peak shows a bimodal distribution and scattering of the molar mass data. A huge error on the calculated molar mass values of PEO 289KDa shown in Table 4.11 might have been caused by polymer adsorption onto the membrane. The concentration

of the polymer that eluted between an elution volume of 10-13 ml was too low to be detected by the RI detector (Fig. 4.24a). When analysing the sample by Thermal FFF, experimental molar mass values close to the nominal values were obtained because no interaction occurred due to the absence of a membrane. Therefore, it can be concluded that PEO is best characterized in organic solvents by Thermal FFF. Analysis of PEO homopolymers was also attempted in ACN and again the polymer strongly adsorbed, such that no meaningful results could be obtained.

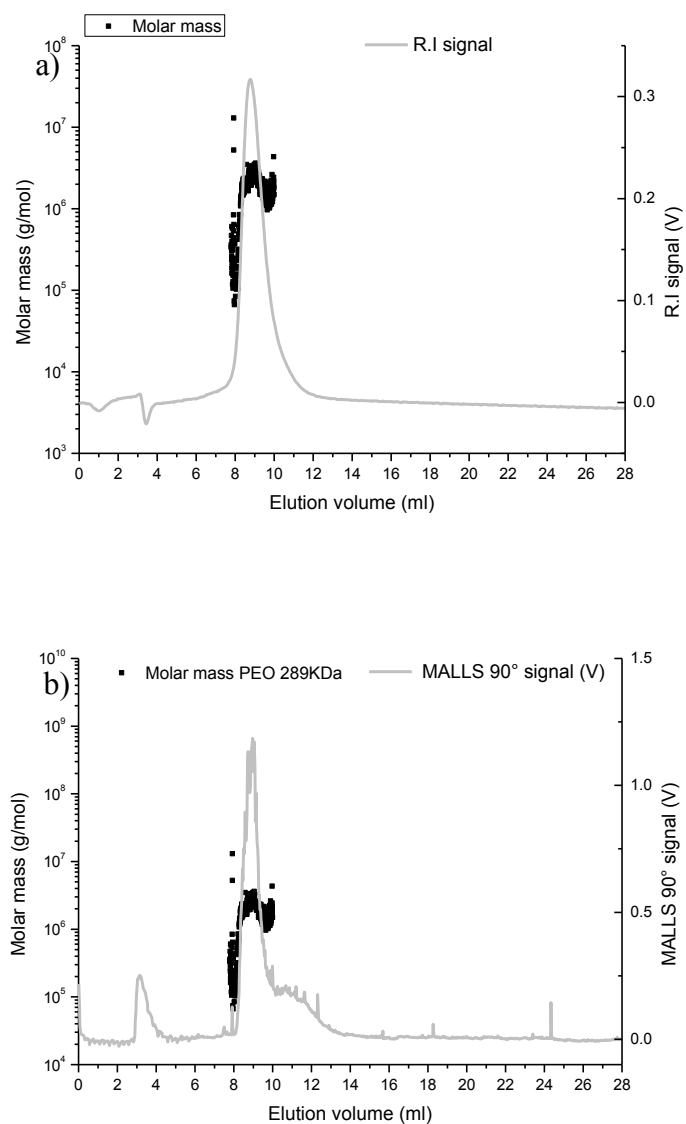


Fig. 4.24 AF4 fractograms in chloroform (a) RI signal with molar mass overlaid and (b) MALLS 90° signal with molar mass overlaid. Sample PEO 289 KDa.

The fractograms in Figs. 4.25a and b show the elution behaviour of PS-b-PEO 218 kDa copolymer and PS 275 kDa. As expected only partial separation occurred. Separation in AF4 is a result of different hydrodynamic radii and sizes in solution^{7, 26, 27}. The peaks closely overlap due to slight differences in the molar masses of the polymers. The PEO 289 kDa fractogram showed strong adsorption on the regenerated cellulose membrane and a very noisy molar mass reading. Unlike in AF4, PEO 289 kDa, PS 275 kDa and PS-b-PEO 218 kDa copolymer were separated in Thermal FFF due to differences in chemical composition (see Figs 4.5a and b). In Thermal FFF no adsorption of the PEO homopolymers occurred due to the absence of a membrane. The molar mass plot of PS-b-PEO 218kDa copolymer shows a rather unusual behaviour: first a decrease in molar mass with increase in elution volume is observed followed by an increase in molar mass with increase in elution volume. This might be due to a bimodal molar mass distribution that appears as a monomodal peak in the RI and MALLS (Figs 4.25a and b). The observed monomodal peaks could be a result of the co-elution of polymers with different molar masses.

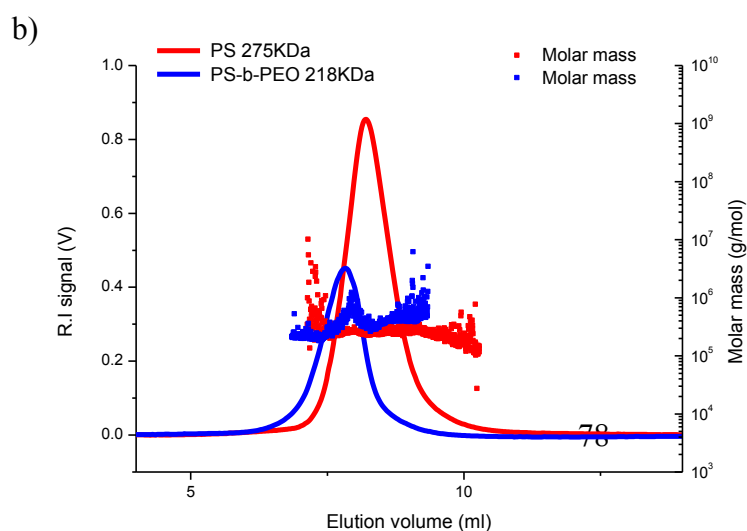
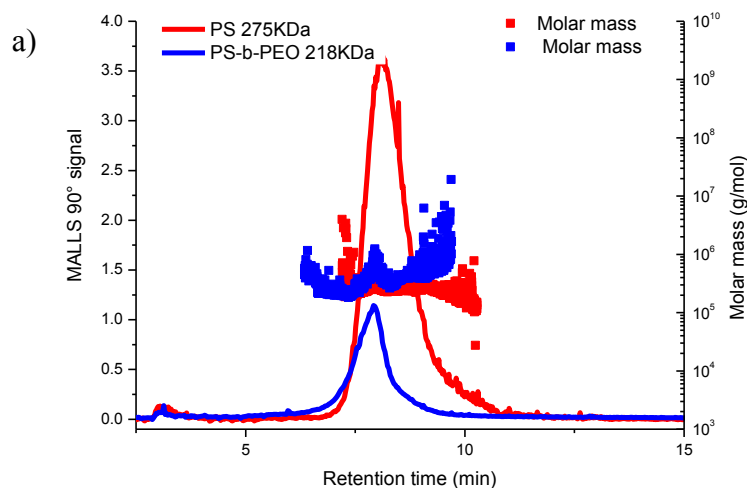
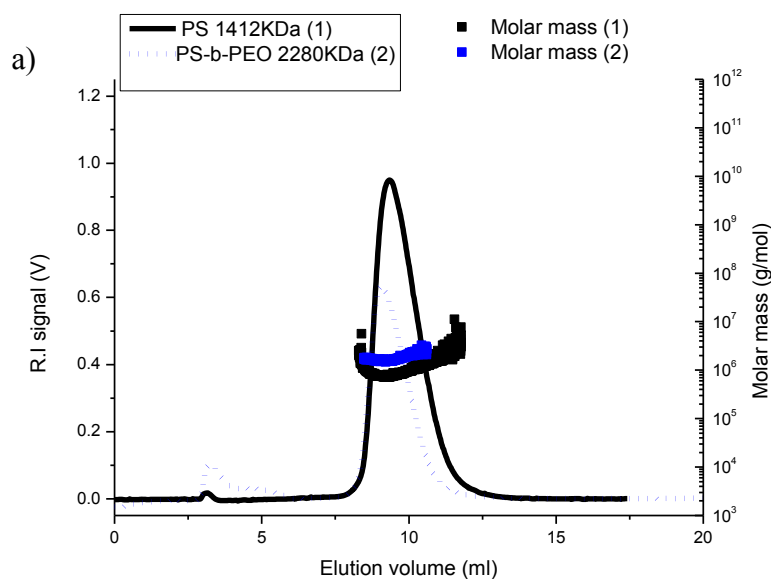


Fig. 4.25 AF4 fractograms in chloroform (a) RI signal with molar mass overlaid and (b) MALLS 90° signal with molar mass overlaid. Samples PS 275 kDa and PS-b-PEO 218 kDa copolymer.

Figs. 4.26a and b show PS-b-PEO 2280 KDa copolymer and PS 1412KDa homopolymer. PS 1412 KDa homopolymer has a molar mass close to the PS block in the block copolymer. The peaks closely overlap. No separation of the polymers occurred; this might have been due to similar hydrodynamic size in solution. As mentioned earlier separation in AF4 is only based on size unlike. In Thermal FFF separation occurred as a result of differences in chemical composition. The Fractograms in Figs 4.26a and b clearly show the adsorption of PS-b-PEO 2280 KDa copolymer. This is as expected since it contains a PEO block with a high molar mass that adsorbs on the regenerated cellulose membrane as described above.



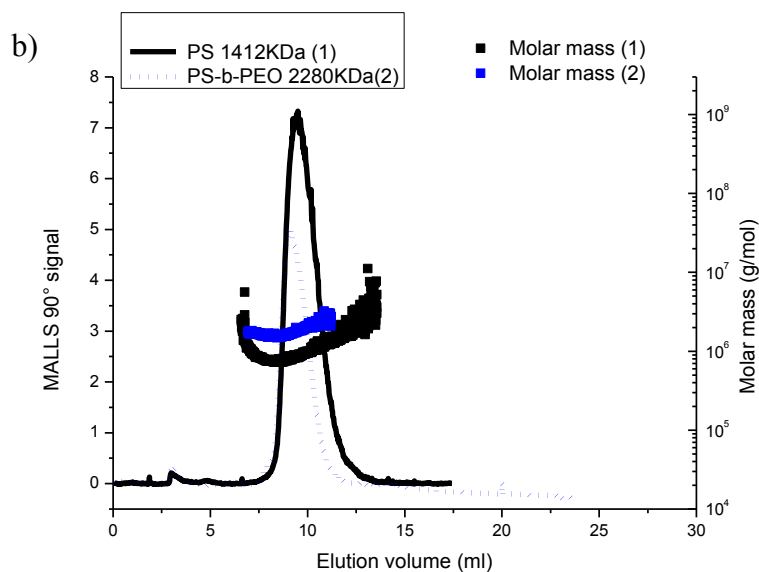


Fig. 4.26 AF4 fractograms in chloroform (a) RI signal with molar mass overlaid and (b) MALLS 90° signal with molar mass overlaid. Samples PEO 1015 kDa, PS-b-PEO 2280 kDa copolymer and PS 1412 kDa.

Reference

1. Runyon, J. R.; Williams, S. K. R. *J. Chromatogr., A* **2011**, 1218, (38), 6774-6779.
2. Sisson, R. M.; Giddings, J. C. *Anal. Chem.* **1994**, 66, (22), 4043-4053.
3. Van Asten, A. C.; Kok, W. T.; Tijssen, R.; Poppe, H. J. *Polym. Sci., Part B: Polym. Phys.* **1996**, 34, (2), 283-295.
4. Martin, M.; Reynaud, R. *Anal. Chem.* **1980**, 52, (14), 2293-2298.
5. Martin, M.; Garcia-Martin, S.; Hoyos, M. *J. Chromatogr., A* **2002**, 960, 165-174.
6. Giddings, J. C.; Myers, M. N.; JanÅ•a, J. *J. Chromatogr., A* **1979**, 186, 37-44.
7. Messaud, F. A.; Sanderson, R. D.; Runyon, J. R.; Otte, T.; Pasch, H.; Williams, K. S. R. *Prog. Polym. Sci.* **2009**, 34, 351-368.
8. Roda, B.; Zattoni, A.; Reschiglian, P.; Moon, M. H.; Mirasoli, M.; Michelini, E.; Roda, A. *Anal. Chim. Acta* **2009**, 635, (2), 132-143.
9. Gunderson, J. J.; Giddings, J. C. *Anal. Chim. Acta* **1986**, 189, 1-15.
10. Podzimek, S., Polymers. In *Light Scattering, Size Exclusion Chromatography and Asymmetric Flow Field Flow Fractionation*, John Wiley & Sons, Inc.: 2011
11. Gunderson, J. J.; Giddings, J. C. *Macromolecules* **1986**, 19, (10), 2618-2621.
12. Kassalainen, G. E.; Williams, K. S. R. *Anal. Chem.* **2003**, 75, (8), 1887-1894.
13. Batten, C.; Hoyos, M.; Martin, M. *Chromatographia* **1997**, 45, (1), 121-126.

14. Jeon Sun, J.; Schimpf Martin, E., Cross-Fractionation of Copolymers Using SEC and Thermal FFF for Determination of Molecular Weight and Composition. In *Chromatography of Polymers*, American Chemical Society: 1999; Vol. 731, pp 141–161.
15. Shiundu, P. M.; Williams, P. S.; Giddings, J. C. *J. Colloid Interface Sci.* **2003**, 266, (2), 366–376.
16. Shiundu, P. M.; Giddings, J. C. *J. Chromatogr.*, **A1995**, 715, (1), 117–126.
17. Runyon, J. R.; Williams, S. K. R. *J. Chromatogr.*, **A 2011**, 1218, (39), 7016–7022.
18. Reschiglian, P.; Zattoni, A.; Roda, B.; Michelini, E.; Roda, A. *Trends Biotechnol.* **2005**, 23, (9), 475–483.
19. Benincasa, M.-A.; Caldwell, K. D. *J. Chromatogr.*, **A 2001**, 925, 159–169.
20. Giddings, J. C.; Caldwell, K. D.; Myers, M. N. *Macromolecules* **1976**, 9, (1), 106–112.
21. Kirkland, J. J.; Yau, W. W. *Macromolecules* **1985**, 18, 2305–2311.
22. Schimpf, M. E. *J. Chromatogr.* **1990**, 517, 405–421.
23. Shiundu, P. M.; Munguti, S. M.; Williams, S. K. R. *J. Chromatogr.*, **A 2003**, 983, 163–176.
24. Malik, M. I.; Harding, G. W.; Grabowsky, M. E.; Pasch, H. *J. Chromatogr.*, **A 2012**, 1244, 77–87.
25. Prestel, H.; Schott, L.; Niessner, R.; Panne, U. *Water Res.* **2005**, 39, (15), 3541–3552.
26. Wittgren, B.; Wahlund, K.-G. *J. Chromatogr.*, **A 1997**, 791, 135–149.
27. Otte, T.; Pasch, H.; Macko, T.; Brúll, R.; Stadler, F. J.; Kaschta, J.; Becker, F.; Buback, M. *J. Chromatogr.*, **A 2011**, 1218, (27), 4257–4267.

Chapter 5:

Conclusions and future work

5.1 Conclusions

Field-flow fractionation is an interesting alternative technique to column-based fractionations. In FFF, separations are conducted in an empty channel applying an external field. The absence of a stationary phase enables the fractionation of sensitive or very high molar mass analytes or analytes that strongly interact with stationary phases.

The present work addresses the behaviour of complex polymers in solvents of different thermodynamic quality. As a typical example, PS-*b*-PEO copolymers were investigated and their solution behaviour compared to the corresponding homopolymers. PS-*b*-PEO copolymers are amphiphilic macromolecules, the PS block being lipophilic and the PEO block being hydrophilic. Such block copolymers may adopt different conformations in solution depending on the solvent quality.

In good solvents for PS like toluene and THF, PEO showed poor solubility. In both THF and toluene retention of PS-*b*-PEO copolymers was dependent on the molar mass of the PS block. This was due to the fact that PS expands freely whilst PEO in Thermal FFF adopts a rather

collapsed coil confirmation which does not contribute significantly to the block copolymer normal diffusion coefficient (D). This led to the co-elution of the PS-*b*-PEO copolymers with PS homopolymer of a molar mass close to that of the PS block in PS-*b*-PEO block copolymer. It was shown that in a good solvent for one block present in a block copolymer the normal diffusion coefficient (D) values are independent of the block copolymer molar mass, but dependent on the molar mass of the block that properly dissolves in the selected solvent. This was evidenced by the D values of PS-*b*-PEO block copolymers which varied insignificantly with those of the PS homopolymers whose molar mass values were close to the molar mass values of the PS blocks in the block copolymers.

Some PS-*b*-PEO copolymers synthesized by sequential living anionic polymerization contained PS and PEO homopolymers as by-products. FTIR spectroscopy was used to qualitatively determine the chemical composition of fractions obtained by semi-preparative Thermal FFF fractionation from some of the PS-*b*-PEO copolymers. When using different solvents different by-product fractions were obtained for the same PS-*b*-PEO copolymers. Therefore it can be concluded Thermal FFF can separate polymers with different chemical compositions as well as different molar masses. In chloroform, a good solvent for both PS and PEO, separation of different polymers was a result of differences in chemical composition.

Based on the investigation of the Thermal FFF elution behaviour of PS homopolymers in toluene, THF and chloroform as well as PEO homopolymers in chloroform, it can be concluded that the homopolymers were separated with regard to their molar mass in the same solvent. The combination of Thermal FFF-DLS-MALLS-UV-RI allowed the online determination of D values and this enabled the calculation of polymer D_T values. Homopolymer normal diffusion coefficients (D) are dependent on molar mass, as shown by the calculated D values for PS, which decreased with increasing molar mass. The D_T values of PS homopolymers with different molar mass values generally varied insignificantly in a given solvent (toluene or THF). This showed that D_T values are dependent on the polymer chemical composition and independent of the molar mass. The homopolymer D_T values varied in different solvent systems as evidenced by the D_T values of PS homopolymers in toluene and THF. Hence these D_T values depend not only on the chemical composition of the polymer but also on the solvent system.

When high constant temperature differences between the cold and hot walls (ΔT) were used, high molar mass polymers were retained for longer periods of time and very broad peaks were obtained. Their fractograms were difficult to analyse in our study. However, the use of a reversed programme temperature gradient allowed the analysis of polymers with molar mass values that span over a wide range in a single experiment, within a short analysis time as well.

When analysing PEO homopolymers with AF4, they strongly interacted with the regenerated cellulose membrane in chloroform. This led to huge errors in the calculation of the molar mass values. PEO analysis in chloroform was however successful in Thermal FFF due to the absence of a regenerated cellulose membrane. PS-b-PEO copolymers interacted with the regenerated cellulose membrane due to the presence of the PEO block.

Based on the results, it can be concluded that Thermal FFF can successfully characterize hydrophilic polymers like PEO in organic solvents such as THF and chloroform due to the absence of a membrane unlike in AF4. PS-b-PEO copolymers can be analysed in Thermal FFF in order to determine their molar mass and chemical composition distribution. In Thermal FFF polymer separation can be a result of differences in molar mass or chemical composition. However in AF4 polymer separation is a result of differences in hydrodynamic size or molar mass only.

5.2 Future work

In future the use of binary solvent combination such as THF/chloroform to dissolve and analyse PS-b-PEO copolymers behaviour would be interesting. The use of a constant ΔT in chloroform in order to quantitatively determine the D_T values of PEO and PS-b-PEO copolymers can be done. The effect of concentration on polymer retention in both Thermal FFF and AF4 could be investigated. In Thermal FFF the optimum concentration can be found in which peak broadening is greatly minimized. Solvent combinations such as water/THF which allow the formation of micelles can be used. Thermal FFF and AF4 can then be used to separate the different polymeric structures formed since FFF is a suitable technique for the fractionation of sensitive polymeric micelles with different size distribution due to the absence of a column.

